Expression and Characterization of HgcA and HgcB, Two Proteins Involved in Methylmercury Biosynthesis

by

Katherine Warfield Rush

A dissertation submitted in partial fulfillment
of the requirements for the degree of
Doctor of Philosophy
(Chemical Biology)
in the University of Michigan
2018

Doctoral Committee:

Professor Stephen W. Ragsdale, Chair
Professor Nicolai Lehnert
Professor Vincent Pecoraro
Professor Janet Smith

Katherine W. Rush

kwrush@umich.edu

ORCID iD: 0000-0001-6842-9055

For my Nana,

Betsy Lee Rush

Acknowledgements

The Ragsdale laboratory has been an amazing place to learn. The first of many thank you's must go to Prof. Stephen Ragsdale, who has allowed me tremendous independence to pursue an unestablished project and given freely of his time, guidance, and support. I feel very lucky to have him as a mentor. I'm extremely grateful for the guidance and friendship of Dr. Angela Fleischhacker and Dr. Eric Carter, who gave so much of their time to teaching me. I've had wonderful discussions on science and life with Dr. Mehmet Can, Dr. Anjali Patwardhan, Dr. Johanna Mock, and Marco Hornung, and to Seth Wiley, pizza artisan/EPR master/climbing buddy/cleric - thank you for making our corner of the lab both thoughtful and hilarious. I also would like to acknowledge an undergraduate colleague, Mohamad Awada, whose work contributed to the results in Chapter 3. I've been privileged to learn from him and all members of the Ragsdale lab my time has coincided with: Dr. Andrea Spencer, Dr. Thanyaporn Wongnate, Heather Aman, Dr. Dariusz Sliwa, Erika Martinez-Nieves, Dr. Panu Pimviriyakul, Liu Liu, Daniel Esckilsen, Dr. Rodney Burton, and Dr. Anindita Sarkar.

This thesis work was conducted in close collaboration with exceptional colleagues at Oak Ridge National Laboratory: Dr. Swapneeta Date, Dr. Liyuan Liang, Dr. Jerry Parks, Dr. Stephen Tomanicek, and Dr. Alexander Johs, whom I am particularly indebted to as my undergraduate research supervisor and long-time source of encouragement. I've gained another incredible mentor teaching Biochemistry 452 with Prof. Alex Ninfa, and I hope to teach one day with his enthusiasm for both good science and good people.

At the University of Michigan, I'd like to thank the incredibly smart members of my cohort within the Program in Chemical Biology, especially my future alpaca farm co-founder, Dr. Oleta Johnson. My thesis committee members, Prof. Nicolai Lehnert, Prof. Vincent Pecoraro, and Prof. Janet Smith, have offered many constructive comments over the course of this work, for which I am grateful. Important Ann Arbor friends I've been lucky to make include Tom Jurkiw, Sarah O'Brien, Dr. Zohar Strinka, James Annand, Sarah Haynes, Paul Campbell, Dr. Jax Sanders, and John Deisinger.

Throughout this process, I've been privileged to have the constant and unconditional support of my family: Dad, Kara, Molly, Big Daniel, Zoë, Little Daniel, Nana, Jim, and Maggie Shults (who may as well be family). I need to include a few special thank you's: to Wally and Derby, my sweet dogs, whose insistence on many long walks around Ann Arbor keeps me happy and healthy. To my father, Greg Rush, who has never told me I am incapable of anything. To Jared – I don't know how to thank you for all the ways you make everything wonderful. Finally, this work is dedicated to my Nana, Betsy Rush. For these 5 years (and all the ones before), she has kept up on my weather forecast, provided and packed the moving truck, and set an example of love and strength for me to follow.

Table of Contents

List of Tables

List of Figures

List of Abbreviations

[4Fe-4S] – four-iron four-sulfur cluster
Ala – alanine
Cbl – cobalamin
CFeSP – corrinoid-iron sulfur protein
Co – cobalt
Cys – cysteine
DMB – dimethylbenzimidazole
EPR – electron paramagnetic resonance
Fe – iron
FL – full-length
Hg – mercury
His – histidine
LIC – ligation-independent cloning
MBP – maltose binding protein
MeCbl – methylcobalamin
MeHg – monomethylmercury
MetH – methionine synthase
Methyl-THF – methyltetrahydrofolate
MHB – MBP-HgcB
SAM – S-adenosylmethionine
Ser – serine
SRB – sulfate-reducing bacteria
TM – transmembrane
TNB – 2-nitro-5-thiobenzoate

Abstract

Methylmercury biosynthesis is a biologically-mediated process linked to expression of the recently discovered *hgcAB* gene products. The environmental conversion of toxic Hg(II) to MeHg, which exhibits even greater biological toxicity, is of concern to ecological food webs and piscivorous human populations. The mechanism by which HgcA and HgcB are responsible for Hg(II) methylation is unknown, but may represent a departure from canonical enzymatic methylation via carbocation mechanisms. The *hgcAB* genes are always found in genomic proximity to one another and predicted to interact within distances amenable to electron transfer in the proposed mechanism of Hg methylation. HgcA is a 40kDa protein comprised of cytosolic and transmembrane domains; the cytosolic domain is predicted to bind a cobalamin cofactor, based on its sequence homology to a known cobalamin-binding protein, which is suggested to serve as the catalytic center of the mercury methylation reaction. HgcB contains two [4Fe-4S] clusters and three additional conserved cysteine residues which we hypothesize are responsible for binding divalent mercury.

No *in vitro* study of HgcA or HgcB has yet been conducted to our knowledge, and this dissertation presents the first protocols for the heterologous expression of both HgcA and HgcB. HgcA contains a C-terminal transmembrane domain and both proteins contain metal cofactors which present significant barriers to heterologous production; thus, *Escherichia coli* cell lines containing co-expression plasmids for cofactor assembly were constructed to circumvent these challenges. In Chapter 2, the HgcB protein was expressed and purified as a maltose-binding protein fusion with 2 iron-replete [4Fe-4S] clusters, as determined by UV-visible and EPR spectroscopic techniques. A series of HgcB variants were constructed containing alanine or serine substitution of the cysteine residues hypothesized to comprise a mercury binding site. The mercury binding characteristics of these variants were probed using stopped-flow rapid kinetics and the results indicated agreement with the requirement for cysteine 73 and either cysteine 94 or 95 observed *in vivo*. This study (a) indicates that these C-terminal cysteine residues are involved in the interaction of HgcB and mercury, and (b) establishes a production system to facilitate

further exploration of this role. It was found in Chapter 3 that truncated HgcA constructs lacking the C-terminal binding domain are not competent to bind cobalamin cofactor. The full-length HgcA protein was expressed in the presence of high intracellular cobalamin and preliminary UV-visible characterization of the holo-FL-HgcA protein is presented. This expression and purification method comprises the critical first step toward *in vitro* validation of the functionality of HgcA as a mercury methylase, as well as the finding that the C-terminal transmembrane domain of HgcA is required for cofactor binding. These studies provide the first characterization of purified HgcA and HgcB, components of a biological system with the puzzling role of synthesizing highly toxic MeHg.

Chapter 1 Introduction to Biological Methylation of Mercury

1.1 Mercury and methylmercury in health and the environment

Mercury (Hg) is a trace metal which exhibits high biological toxicity[1]. It is estimated that one-third[2] to two-thirds[3] of yearly Hg inputs into the environment are anthropogenic in origin, primarily due to coal combustion and industrial process waste; other environmental deposition is geologic in origin. Elemental Hg(0) is liquid at room temperature, thus its environmental cycling is controlled by complex atmospheric equilibria at the air-water interface. Hg(0) is deposited into aquatic systems from the atmosphere, where it is subject to redox processes and methylation/demethylation equilibria as shown in Figure 1.1[4]. Inorganic Hg(II) is highly toxic and causes acute kidney failure in vertebrates at low doses[1], though its exact mechanisms of toxicity are poorly understood across kingdoms of life. It is thought that Hg biological trafficking and toxicity are the result of the high affinity of Hg(II) for thiolate coordination. Monomethylmercury (MeHg) is a neurotoxin and bioaccumulates within the aquatic food web, with high MeHg concentrations found in fish, bird, and mammal species at high trophic levels[5]; this occurs due to the propensity of MeHg to cross the blood-brain barrier.

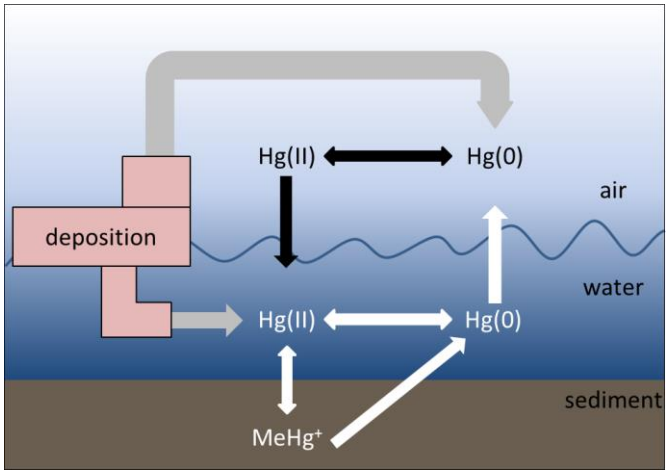

Figure 1.1 Schematic depiction of relevant equilibria in the Hg biogeochemical cycle. Hg(0) and Hg(II) deposition into the environment results in a complex global cycle across the

atmosphere-water interface. Hg(II) undergoes biologically-mediated methylation and demethylation at the sediment-water interface. Adapted from Reference 1.

Methylation of environmental Hg increases with increased atmospheric deposition[6], and rising MeHg levels are a serious threat to fish-consuming human populations[2]. Processes such as permafrost thaw[7], which is of immediate concern due to high levels of Hg accumulation in Arctic environments affected by global climate change, can also cause a rapid increase in an ecosystem's Hg methylating activity. Curiously, neurotoxic MeHg is biosynthesized by microorganisms – that is, a biologically mediated process exists which converts toxic Hg(II) to the more toxic MeHg, neither of which are known to serve any advantageous biological function. Biological methylation of Hg was first proposed in 1969, after observing that, though the dominant Hg species in aquatic environments is inorganic Hg(II), MeHg is the species which accumulates in fish tissue[8]. Metabolic inhibitors against various classes of organisms identified sulfate-reducing bacteria (SRB) as the primary Hg methylators[9] and radiocarbon labelling studies linked MeHg biosynthesis to serine and folate metabolisms and implicated the involvement of a methylcobalamin (MeCbl) cofactor[10]. Choi and Bartha conducted a series of studies investigating this link in the early 1990's, indicating that generation of MeHg is likely enzyme-catalyzed rather than an abiotic reaction of free MeCbl[11] and identifying a 40kDa corrinoid protein in a *Desulfovibrio* species as a putative methylase using a series of ^{57}Co and ^{14}C radolabelling studies[12], but little additional information on the biochemical pathway by which bacterial Hg methylation proceeds was published until 2013.

1.2 *hgcAB*-linked mercury methylation

Parks *et.al.*[13] used a bioinformatics approach to search the genomes of known Hg methylators for a common, cobalamin-dependent methyltransferase, and identified the *hgcAB* genes as biomarkers of Hg methylation capability. At the time of this discovery, four species of SRB and two species of the genus *Geobacter* were known to methylate Hg in monoculture. Establishing a genetic link to the Hg-methylating phenotype led to the identification of an additional 46 Hg methylators across the kingdoms of *Bacteria* and *Archaea*, and this number has since grown to over 200 species containing homologs of *hgcAB*[14].

A phylogenetic analysis conducted in 2013 grouped the 70 *hgcAB* gene clusters found in available genomes into 5 clades: three among *Deltaproteobacteria* (including every species of *Geobacter*, save one), methanogens within *Euryarchaeota*, and *Clostridia*[15]. This work solidified

the link between Hg methylation capability and *hgcAB* by showing that *hgcAB*$^-$ close evolutionary relatives of a variety of *hgcAB*$^+$ organisms cannot methylate Hg, whereas all tested *hgcAB*$^+$ organisms do methylate Hg; this definitively showed that MeHg biosynthesis requires the *hgcAB* genes. The authors of this study emphasize that the vast diversity of newly identified Hg methylating organisms necessitates an expansion of Hg methylation study to previously unrecognized environmental niches, including those in which the dominant Hg methylators are methanogenic *Archaea*: these include rice paddies[16], permafrost and Arctic sediments[17], and freshwater aquatic systems[18].

Methanogens have recently been shown to methylate Hg at similar rates to SRB and iron-reducing bacteria when those rates are adjusted for total cell protein[14], in contrast to older reports that these species were not significant contributors to environmental Hg production[9]. Syntrophic effects on Hg methylation are an area of exploration which have also benefited from the identification of the *hgcAB* biomarkers; synergistic growth between Hg-methylating SRB and methanogens was first observed in 1998[19], and a recent report has shown stimulation of MeHg production in environmentally relevant combinations of Hg-methylating organisms with syntrophic metabolic relationships[20]. One niche in which the *hgcAB* genes are conspicuously absent, as determined in a large-scale study of metagenomes[17], is the vertebrate digestive microbiome – this suggests that human inorganic Hg exposure is not exacerbated by conversion to neurotoxic MeHg within the body.

Two nonexclusive hypotheses exist concerning evolutionary advantages which the *hgcAB* genes may provide. One is that these genes confer some resistance to Hg(II) toxicity; this does not appear to be the case in *hgcAB*$^+$ organisms, based on cell growth rates in the presence or absence of Hg in *Desulfovibrio desulfuricans* ND132 and nearby genetic relatives[21]. This study, however, was conducted on a limited number of organisms before the identification of the *hgcAB* gene cluster and is not conclusive. It should be noted that methylmetals of arsenic, tin, and selenium are formed by microbial processes and thought to protect against the toxic effects of these elements by increasing their volatility and membrane permeability[22–24], and this possibility cannot yet be eliminated for MeHg. The other conceivable function of HgcA and HgcB is that they catalyze some methyl transfer process associated with cellular carbon metabolism and methylate Hg(II) adventitiously as a side product. This is supported by two findings from global proteome studies: addition of Hg(II) to cultures of *Desulfovibro desulfuricans* ND132 did not

induce a change in the expression levels of HgcA and HgcB[25], and a lower abundance of genes involved in the folate branch of the acetyl-CoA pathway was observed in a *hgcAB* deletion mutant of *Geobacter sulfurreducens* PCA[26]. At the time of this writing, no decisive work has been conducted to directly interrogate other metabolic functions of the *hgcAB* genes. In summary, study of HgcA and HgcB is just beginning and no conclusions can yet be drawn as to their biological role.

As HgcA is a cobalamin-dependent methyltransferase, this introductory chapter will review the known cobalamin-dependent abiotic and enzymatic methyl transfer processes. The putative roles of HgcB in both electron transfer through its iron-sulfur clusters and Hg binding via a cysteine-rich, high-affinity Hg(II) binding site will be also discussed. Finally, the proposed catalytic cycle for methyl transfer to Hg(II) and open questions will be presented as they relate to the scope of this dissertation research.

1.3 Methylcobalamin and mechanisms of mercury methylation

Cobalamin (Cbl), the structure of which is shown in Figure 1.2, is comprised of a cobalt atom coordinated by the 4 nitrogen atoms of the macrocyclic corrin ligand[27]. It is unique among tetrapyrroles in the addition of an intramolecular 5th ligand to the central cobalt which is covalently attached to the α-face of the macrocycle via a nucleotide linkage[28]. This axial base ligand is dimethybenzimidazole (DMB) in Cbl and not present in cobinamide (Cbi); the term "corrinoid" captures both of these compounds as well as those containing other base moieties. The Cbl cobalt center can access the +1, +2, and +3 oxidation states, and thus transfer alkyl cation, radical, and anion species[29]. In a 1974 review of toxic element cycles in the environment[23], Wood discusses methylation of Hg(II) by methylcobalamin (MeCbl) as an early mechanistic hypothesis for MeHg biosynthesis, simply because of this capacity to transfer a methyl anion or radical. Reactions of other known biological methyl transfer donors, methyltetrahydrofolate (methyl-THF) and S-adenosylmethionine, result in transfer of a methyl cation; this species would be an unlikely ligand for Hg(II) on the basis of electrostatic repulsion.

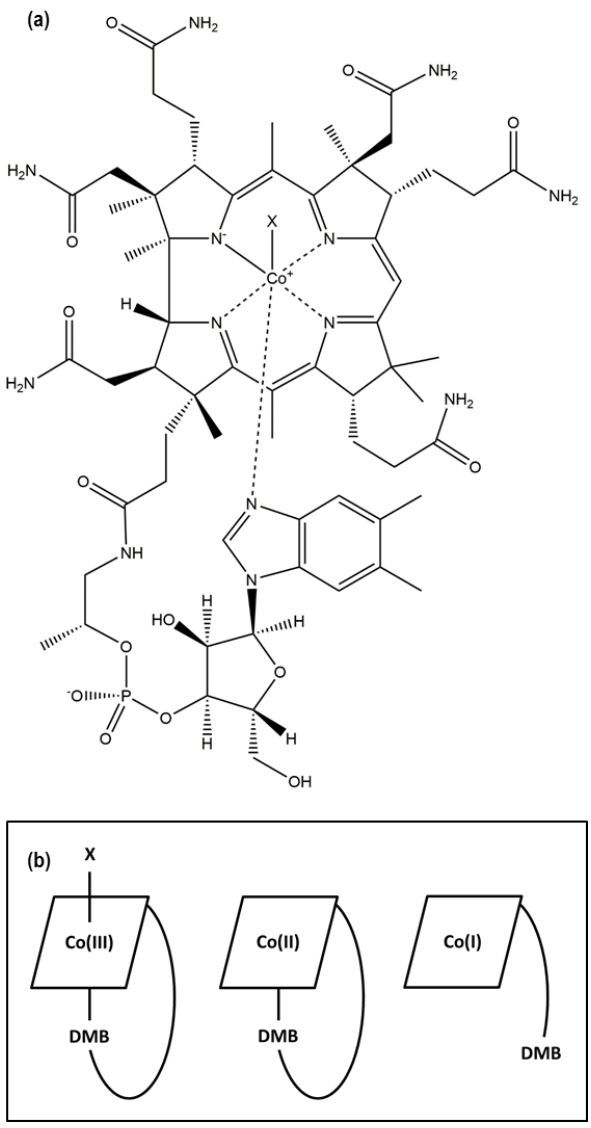

Figure 1.2 Structure of the cobalamin cofactor (a) Structure of the cobalamin cofactor, where X represents an upper axial ligand, such as X = CH_3 in methylcobalamin (b) Representations of the coordination environments of cobalamin in the Co(III), Co(II), and Co(I) states, which assume coordination numbers of 6, 5, and 4, respectively. The planar face containing the Co atom represents the four-coordinate corrin ring, DMB is the base moiety coordinating the α-axial position, and X signifies the more readily exchangeable β-axial ligand.

When MeCbl was connected to MeHg production, it was unknown whether Cbl-mediated Hg methylation was abiotic or enzyme-mediated. Abiotic methylation of Hg by MeCbl is thought to proceed via carbanion transfer to the electrophilic Hg(II), resulting in the products MeHg+ and cob(III)alamin[30]. This reaction has been shown to be faster for cobalamin vs. cobinamide, the latter lacking the dimethylbenzimidazole (DMB) moiety which coordinates the

central Co atom, but also promoted by low pH, which increases the fraction of cobalamin in the "base-off" form due to protonation and weakened affinity of the DMB ligand[31]; this indicates both that DMB has a positive effect on the dealkylation of Cbl by Hg(II) but that its removability is also important in the reaction. Though this mechanism is not yet fully resolved, it has been observed that the abiotic reaction is slow at physiological pH and inhibited when Hg(II) is supplied as a bis-thiolate complex[32]. These findings are significant because intracellular methylation of Hg would presumably occur at near-neutral pH and Hg(II)-thiolate complexes are understood to be the dominant Hg species in cells and the environment[33]. Our knowledge of abiotic Hg methylation by Cbl is therefore consistent with the finding that environmental Hg methylation is, instead, enzymatically mediated by the corrinoid-dependent HgcA.

1.4 HgcA and enzymatic corrinoid-dependent methyl transfer

Cbl enzyme cofactors catalyze an ever-increasing list of biological reactions[34], including methyl group transfer. Well-characterized examples of this process include methionine synthase (MetH)[35] and the corrinoid iron-sulfur protein (CFeSP)[36], which is involved in the Wood-Ljungdahl pathway of microbial acetogenesis. In both of these examples, the ability of the Cbl cofactor to access the Co(I) and Co(III) oxidation states is central to the mechanism of methyl transfer[37]. The "supernucleophilic" Co(I) state is capable of accepting a methyl group to form a Me-Co(III) corrinoid. This methyl group can then be transferred to homocysteine or the acetyl Co-A synthase nickel cluster, in the cases of MetH and CFeSP, respectively. These mechanisms result in the transfer of a methylcation (CH_3^+), and the two electrons comprising the Co-C bond return to the Co to reset the catalytic cycle at the Co(I) state.

Four Cbl protein binding modes for which crystal structures are available are shown in Figure 1.3. Cofactor binding to these enzymes occurs in the "base-off" binding mode, in which the lower axial DMB moiety dissociates from the central Co atom and binds via contacts to a protein Rossmann fold. In the case of MetH, th base is replaced by a protein His ligand[35]; CFeSP lacks a lower axial Cbl ligand, and instead binds via a "base-off" mode[36]. The recently characterized transcriptional regulator CarH similarly binds a cobalamin cofactor and provides two protein His ligands in a "base-off, bis-His" configuration reminiscent of common heme binding motifs[38]. Homology modelling based on sequence similary to the CFeSP suggests the cytosolic domain of HgcA, comprising ~18kDa of the 40kDa polypeptide, binds a corrinoid

cofactor in the "base-off, Cys-on" conformation through a Rossmann fold motif and coordination to the cobalt through Cys73[13]. A recent structural study has identified a "base-off, Cys-on" Cbl binding mode in a structure of a membrane associated corrinoid transport protein, BtuM[39]. This Cys residue, however, is suggested to catalyze decyanation of cyano-Cbl, and this enzyme does not appear to be involved in methyl transfer. Therefore, no system is known which provides an example of the effect of a lower axial Cys ligand on Co-C bond cleavage.

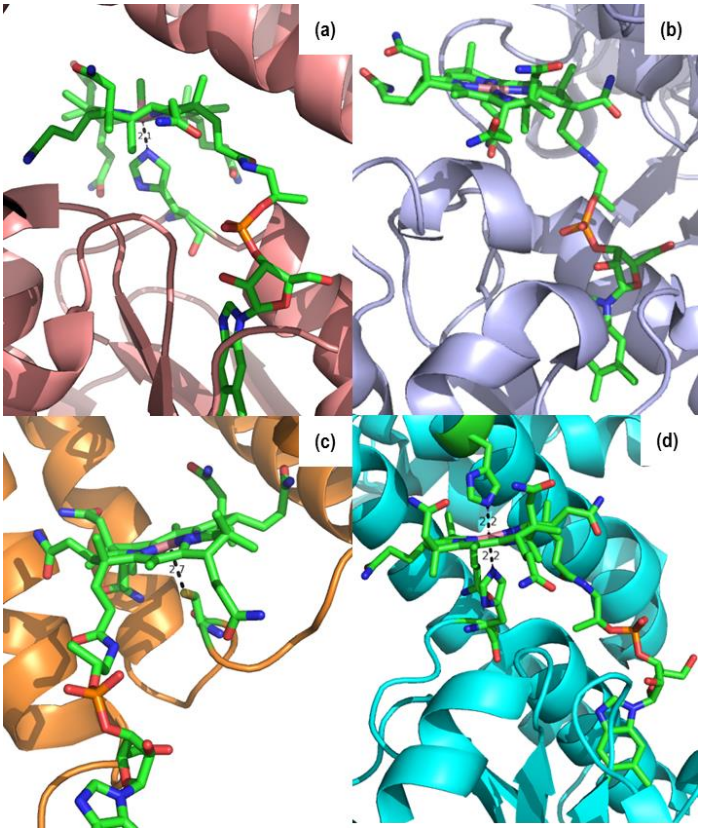

Figure 1.3 Crystal structures of observed "base-off" cobalamin protein binding modes (a) "base-off, His-on" methionine synthase (MetH) (b) "base-off" corrinoid iron-sulfur protein (CFeSP) (c) "base-off, Cys-on" vitamin B12 membrane transporter (BtuM) (d) "base-off, bis-His" light-dependent transcriptional regulator (CarH). The proteins are represented as colored cartoons while the cobalamin and relevant protein ligands are represented as sticks and colored by element. Rendered with Pymol from Protein Data Bank entries (a) 1BMT, (b) 4DJD, (c) 6FFV, and (d) 58CF.

Cys73 is strictly conserved among *hgcA* genes, has been shown to be critical to Hg methylation *in vivo*[40], and is hypothesized to have a dramatic effect on corrinoid-dependent methyl transfer via HgcA. Zhou et.al. constructed density functional theory calculations to model the *trans* effect of a thiolate ligand on Co-C bond cleavage[41]. They determined that a "base-off, Cys-on" Cbl coordination mode should modulate the bond dissociation energy of the Co-C bond

such that heterolysis releasing a carbanion (CH_3^-) would be the energetically preferred mode of bond dissociation. Though the local protein environment could modulate this and experimental validation is necessary, this model provides a chemical rationale for the departure of HgcA from known mechanisms of enzymatic carbocation transfer and supports the mechanistic hypothesis first proposed in Parks et.al.[13] (it should be noted that, though not observed in an enzymatic system, carbanion transfer is suggested in the abiotic methylation of Hg as discussed in section 1.3, so this is not a corrinoid reaction without chemical precendent). In this mechanism, the HgcA corrinoid would first assume the Co(I) state to generate Me-Co(III) with an unknown methyl donor, then methyl transfer to the strongly electrophilic Hg(II) would result in a Co(III) corrinoid, with a requirement for reduction to Co(I) to reset catalysis. Essential to this process is the donation of two electrons every cycle to return the Co to the Co(I) state; this is the hypothesized role of HgcB.

1.5 Mercury binding and HgcB, a [4Fe-4S] cluster ferredoxin-like protein

HgcB is a 10kDa ferredoxin-like protein which contains two four-iron four-sulfur ([4Fe-4S]) cluster CXXCXXCXXXCP consensus motifs. [4Fe-4S] clusters are an ancient and ubiquitious biological feature known to store and transfer low potential electrons[42], and it is hypothesized that the HgcB iron-sulfur (Fe-S) clusters are responsible for 2-electron reduction of the Co(III) HgcA corrinoid after carbanion transfer. In the "base-off" CFeSP, the Co(II)/Co(I) midpoint redox potential is increased from the "base-on" potential of ~600mV to ~450mV[43]. We have no information on the Co(II)/Co(I) redox couple in HgcA, as this will be dependent on its coordination state, binding mode, and protein environment, but we anticipate that the HgcB clusters will exhibit sufficiently low midpoint potentials to reduce the corrinoid species. In addition to the 8 Cys residues involved in the Fe-S clusters, HgcB contains 3 strictly conserved Cys residues: Cys73, Cys94, and Cys95, with Cys94 and Cys95 occupying the C-terminus. Hg(II) has an strong preference for thiolate coordination, and it has been proposed that these Cys residues comprise a high-affinity Hg(II) binding site[13]. This could facilitate catalysis by positioning the Hg(II) in a favorable proximity for methylation. Peptide studies have shown that vicinal Cys residues are highly specific for Hg(II) binding over other thiophilic divalent metal ions, compared to CAAC and CACA motifs[44]. Cys-rich motifs, including those with vicinal Cys

pairs, have been observed and characterized in other Hg(II) binding proteins, notably those found within the *mer* operon.

The *mer* operon encodes genes widespread in aerobic organisms which are responsible for uptake and degradation of MeHg[45]. This pathway involves Hg(II) dependent transcriptional activation by MerR, chaperoned import of Hg(II) or MeHg, cleavage of the Hg-C bond by the organomercurial lyase MerB, and reduction of the resulting Hg(II) to the relatively inert and nontoxic Hg(0) by MerA. All of these processes are mediated by Cys-based Hg(II) binding sites: MerT[46] and MerF[47], membrane Hg(II) transport proteins, contain Cys-Cys vicinal pairs, as do MerB[48] and MerA[49]. A variety of Cys motifs are seen in other *mer* operon binding sites, including an unusual example in the MerR transcriptional regulator, which has been shown to bind Hg(II) with high affinity and specificity in a 3-Cys trigonal planar mode, in contrast to the typically preferred linear geometry[50,51]. An *in vivo* mutagenesis study of HgcA and HgcB in the model Hg methylator *Desulfovibrio desulfuricans* ND132 investigated the impact of alanine (Ala) substitution of the three conserved HgcB Cys residues[40]. These results indicated that Cys73 and either Cys94 or Cys95 are required for *in vivo* Hg methylation activity, but the loss of one of the C-terminal pair can be accommodated. This suggests that some configuration of these residues is required for MeHg production, though *in vitro* characterization of these mutants would be required to confirm that the loss of Hg methylating activity is due specifically to Hg binding deficiency.

1.6 Hypothesized mercury methylation process and scope of this dissertation

Figure 1.4 depicts the hypothesisized *hgcAB*-mediated MeHg biosynthesic scheme presented in Parks et.al. In this model, Co(III)-HgcA is reduced with two electrons transferred from the HgcB [4Fe-4S] clusters and methylated. The methyl-Co(III) corrinoid then transfers a methyl anion to a Hg(II) atom coordinated to HgcB via cysteine ligands, resulting in $MeHg^{+}$ and a Co(III) species at the end of the catalytic cycle. This is a working model constructed using insight from homology modelling[13], computational prediction[41], and *in vivo* mutagenesis[40] studies. Though these have provided some insight into critical features of this process, as described in previous sections of this chapter, *in vitro* investigation is required to directly answer mechanistic questions. Is methylated HgcA capable of methyl transfer to Hg(II)? If so, what is the electronic nature of the methyl group which is transferred to Hg(II)? Does Cys73 coordinate

the HgcA corrinoid cofactor and affect Co-C bond dissociation? Is HgcB required for reduction of the corrinoid? Does it bind and supply the Hg(II) substrate to accelerate catalysis, as well? We suggest that these as-yet uninvestigated questions can be answered by biochemical and spectroscopic characterization of purified HgcA and HgcB.

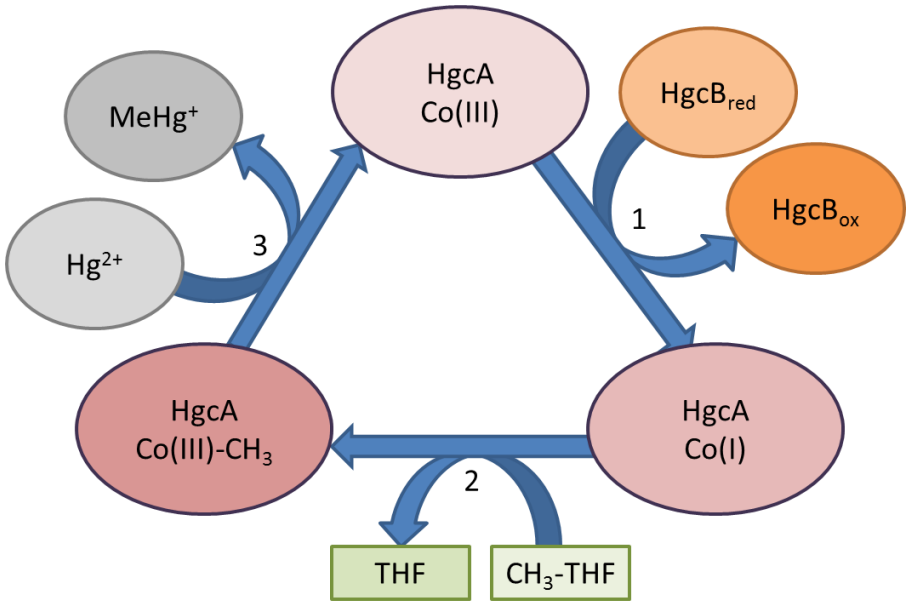

Figure 1.4 Working model of Hg methylation by HgcA and HgcB (1) Reduction of the HgcA corrinoid cofactor by 2-electron transfer from HgcB. It is unknown what electron donor may supply these low-potential electrons. (2) Methylation of Co(I)-HgcA by a methyl donor – this is written as methyltetrahydrofolate as many *hgcAB*+ organisms contain folate metabolic pathways, but it is unknown whether HgcA reacts directly with methyl-THF (3) Methyl transfer to Hg(II) to generate MeHg+ and the inactive Co(III)-HgcA. We hypothesize this Hg(II) is associated with HgcB.

This thesis project was initiated to characterize the newly discovered HgcA and HgcB proteins from *Desulfovibrio desulfuricans* ND132. As no *in vitro* study of HgcA or HgcB has been conducted to date, any knowledge of their features gained in this work will be beneficial to further understanding of biological Hg methylation. Our particular interest in these proteins lies in their diverse metal centers, which are hypothesized to be critical to their novel functions. In Chapter II, UV-visible and electron paramagnetic resonance (EPR) spectroscopic characterization of HgcB was conducted to understand the composition of its predicted [4Fe-4S] cluster motifs. The Hg binding characteristics of a panel of HgcB Cys variants were probed using a Hg ligand-exchange titration coupled to stopped-flow rapid kinetics – this yielded insight into the *in vivo* functional requirement for Cys73 and either Cys94 or Cys95. In Chapter III, two

approaches were taken to HgcA production: generation of a truncated HgcA constructs to promote soluble heterologous expression and co-expression of the full-length transmembrane protein with a plasmid controlling cellular uptake of cobalamin. The latter technique resulted in the heterologous expression and purification of full-length HgcA, the UV-visible spectrum of which will be presented. These results provide the Hg biotransformation field with preliminary characteristics of these proteins, which will be valuable to further mechanistic understanding of MeHg biosynthesis.

1.7 References for Chapter 1

(1) Clarkson, T. W. Critical Reviews in Toxicology The Toxicology of Mercury and Its Chemical Compounds. *Crit. Rev. Toxicol.* **2006**, *36* (8), 609–662.

(2) Fitzgerald, W. F.; Clarkson, T. W. Mercury and Monomethylmercury: Present and Future Concerns. *Environ. Health Perspect.* **1991**, *96*, 159–166.

(3) Nriagu, J. O.; Pacyna, J. M. Quantitative Assessment of Worldwide Contamination of Air, Water and Soils by Trace Metals. *Nature* **1988**, *333*, 134–139.

(4) Mason, R. P.; Abbott, M. L.; Bodaly, R. A.; Bullock, R.; Driscoll, C. T.; Evers, D. C.; Lindberg, S. E.; Murray, M.; Swain, E. B. Monitoring the Response to Changing Mercury Deposition. *Environ. Sci. Technol.* **2005**, No. 39, 15A–22A.

(5) Evers, D. C.; Clair, T. A. Mercury in Northeastern North America: A Synthesis of Existing Databases. *Ecotoxicology* **2005**, *14* (1–2), 7–14.

(6) Harris, R. C.; Rudd, J. W. M.; Amyot, M.; Babiarz, C. L.; Beaty, K. G.; Blanchfield, P. J.; Bodaly, R. A.; Branfireun, B. A.; Gilmour, C. C.; Graydon, J. A.; et al. Whole-Ecosystem Study Shows Rapid Fish-Mercury Response to Changes in Mercury Deposition. *Proc. Natl. Acad. Sci.* **2007**, *104* (42), 16586–16591.

(7) Yang, Z.; Fang, W.; Lu, X.; Sheng, G. P.; Graham, D. E.; Liang, L.; Wullschleger, S. D.; Gu, B. Warming Increases Methylmercury Production in an Arctic Soil. *Environ. Pollut.* **2016**, *214*, 504–509.

(8) Jensen, S.; Jernelöv, A. Biological Methylation of Mercury in Aquatic Organisms. *Nature* **1969**, *223* (5207), 753–754.

(9) Compeau, G. C.; Bartha, R. Sulfate-Reducing Bacteria: Principal Methylators of Mercury in Anoxic Estuarine Sediment. *Microbiology* **1985**, *50* (2), 498–502.

(10) Berman, M.; Chase, T.; Bartha, R. Carbon Flow in Mercury Biomethylation by Desulfovibrio-Desulfuricans. *Appl. Environ. Microbiol.* **1990**, *56* (1), 298–300.

(11) Choi, S. C.; Bartha, R. Cobalamin-Mediated Mercury Methylation by Desulfovibrio Desulfuricans LS. *Appl. Environ. Microbiol.* **1993**, *59* (1), 290–295.

(12) Choi, S. C.; Chase, T.; Bartha, R. Enzymatic Catalysis of Mercury Methylation by Desulfovibrio Desulfuricans LS. *Appl. Environ. Microbiol.* **1994**, *60* (4), 1342–1346.

(13) Parks, J. M.; Johs, A.; Podar, M.; Bridou, R.; Hurt Jr., R. A.; Smith, S. D.; Tomanicek, S. J.; Qian, Y.; Brown, S. D.; Brandt, C. C.; et al. The Genetic Basis for Bacterial Mercury Methylation. *Science.* **2013**, *339*, 1332–1336.

(14) Gilmour, C. C.; Bullock, A. L.; McBurney, A.; Podar, M.; Elias, D. A. Robust Mercury Methylation across Diverse Methanogenic *Archaea*. *MBio* **2018**, *9* (2), e02403-17.

(15) Gilmour, C. C.; Podar, M.; Bullock, A. L.; Graham, A. M.; Brown, S. D.; Somenahally, A. C.; Johs, A.; Hurt, R. A.; Bailey, K. L.; Elias, D. A. Mercury Methylation by Novel Microorganisms from New Environments. *Environ. Sci. Technol.* **2013**, *47* (20), 11810–11820.

(16) Rothenberg, S. E.; Anders, M.; Ajami, N. J.; Petrosino, J. F.; Balogh, E. Water Management Impacts Rice Methylmercury and the Soil Microbiome. *Sci. Total Environ.* **2016**, *572*, 608–617.

(17) Podar, M.; Gilmour, C. C.; Brandt, C. C.; Soren, A.; Brown, S. D.; Crable, B. R.; Palumbo, A. V.; Somenahally, A. C.; Elias, D. A. Global Prevalence and Distribution of Genes and Microorganisms Involved in Mercury Methylation. *Sci. Adv.* **2015**, *1* (9), 1–12.

(18) Christensen GA, S. A.; Moberly JG, Miller CM, King AJ, G. C.; Brown SD, Podar M, Brandt CC, B. S.;

Palumbo AV, Wall JD, E. DA. Carbon Amendments Alter Microbial Community Structure and Net Mercury Methylation Potential in Sediments. *Appl Env. Microbiol* **2018**, *84* (3), 1–14.
(19) Pak, K. R.; Bartha, R. Mercury Methylation by Interspecies Hydrogen and Acetate Transfer between Sulfidogens and Methanogens. *Appl. Environ. Microbiol.* **1998**, *64* (6), 1987–1990.
(20) Yu, R. Q.; Reinfelder, J. R.; Hines, M. E.; Barkay, T. Syntrophic Pathways for Microbial Mercury Methylation. *ISME J.* **2018**, *12* (7), 1826–1835.
(21) Gilmour, C. C.; Elias, D. A.; Kucken, A. M.; Brown, S. D.; Palumbo, A. V.; Schadt, C. W.; Wall, J. D. Sulfate-Reducing Bacterium Desulfovibrio Desulfuricans ND132 as a Model for Understanding Bacterial Mercury Methylation. *Appl. Environ. Microbiol.* **2011**, *77* (12), 3938–3951.
(22) Carrillo-González, R.; Šimůnek, J.; Sauvé, S.; Adriano, D. Mechanisms and Pathways of Trace Element Mobility in Soils. *Adv. Agron.* **2006**, *91* (06), 111–178.
(23) Wood, J. M. Biological Cycles for Toxic Elements in the Environment. *Science.* **1974**, *183* (4129), 1049–1052.
(24) Nagase, H.; Sato, T.; Yoshioka, Y. Formation, Distribution, and Ecotoxicity of Methylmetals of Tin, Mercury, and Arsenic in the Environment. *Crit. Rev. Environ. Sci. Technol.* **1995**, *25* (1), 45–91.
(25) Qian, C.; Chen, H.; Johs, A.; Lu, X.; An, J.; Pierce, E. M.; Parks, J. M.; Elias, D. A.; Hettich, R. L.; Gu, B. Quantitative Proteomic Analysis of Biological Processes and Responses of the Bacterium *Desulfovibrio Desulfuricans* ND132 upon Deletion of Its Mercury Methylation Genes. *Proteomics* **2018**, 1700479.
(26) Qian, C.; Johs, A.; Chen, H.; Mann, B. F.; Lu, X.; Abraham, P. E.; Hettich, R. L.; Gu, B. Global Proteome Response to Deletion of Genes Related to Mercury Methylation and Dissimilatory Metal Reduction Reveals Changes in Respiratory Metabolism in Geobacter Sulfurreducens PCA. *J. Proteome Res.* **2016**, *15* (10), 3540–3549.
(27) Banerjee, R. V. *Chemistry and Biochemistry of B12*; John Wiley and Sons, 1999.
(28) Banerjee, R.; Ragsdale, S. W. The Many Faces of Vitamin B_{12}: Catalysis by Cobalamin-Dependent Enzymes. *Annu. Rev. Biochem.* **2003**, *72* (1), 209–247.
(29) Schrauzer, G. N. Mechanisims of Corrin Dependent Enzymatic Reactions. In *Fortschritte der Chemie Organischer Naturstoffe/Progress in the Chemistry of Organic Natural Products*; Herz, W., Grisebach, H., Kirby, G. W., Eds.; Springer, Vienna, 1974; pp 583–628.
(30) Hill, H. A. O.; Pratt, J. M.; Ridsdale, S.; Williams, F. R.; Williams, R. J. P. Kinetics of Substitution of Co-Ordinated Carbanions in Cobalt (III) Corrinoids. *J. Chem. Soc. D* **1970**, *124*, 341–341.
(31) DeSimone, R. E.; Penley, M. W.; Charbonneau, L.; Smith, S. G.; Wood, J. M.; Hill, H. A. O.; Pratt, J. M.; Ridsdale, S.; Williams, R. J. P. The Kinetics and Mechanism of Cobalamin-Dependent Methyl and Ethyl Transfer to Mercuric Ion. *Biochim. Biophys. Acta* **1973**, *304*, 851–863.
(32) Bertilsson, L.; Neujahr, M. Y. Methylation of Mercury Compounds by Methylcobalamin. *Biochemistry* **1971**, *10* (14), 2805–2808.
(33) Fretham, S. J. B.; Aschner, M. Mercury. In *RSC Metallobiology Series No. 2: Binding, Transport and Storage of Metal Ions in Biological Cells*; Maret, W., Wedd, A., Eds.; Royal Society of Chemistry, 2014; pp 747–767.
(34) Bridwell-Rabb, J.; Drennan, C. L. Vitamin B12 in the Spotlight Again. *Curr. Opin. Chem. Biol.* **2017**, *37*, 63–70.
(35) Goulding, C. W.; Postigo, D.; Matthews, R. G. Cobalamin-Dependent Methionine Synthase Is a Modular Protein with Distinct Regions for Binding Homocysteine, Methyltetrahydrofolate, Cobalamin, and Adenosylmethionine. *Biochemistry* **1997**, *36* (26), 8082–8091.
(36) Ragsdale, S. W.; Lindahl, P. A.; Munck, E. Mossbauer, EPR, and Optical Studies of the Corrinoid/Iron-Sulfur Protein Involved in the Synthesis of Acetyl Coenzyme A by Clostridium Thermoaceticum. *J. Biol. Chem.* **1987**, *262* (29), 14289–14297.
(37) Matthews, R. G.; Koutmos, M.; Datta, S. Cobalamin-Dependent and Cobamide-Dependent Methyltransferases. *Curr. Opin. Struct. Biol.* **2008**, *18* (6), 658–666.
(38) Jost, M.; Fernandez-Zapata, J.; Polanco, M. C.; Ortiz-Guerrero, J. M.; Chen, P. Y. T.; Kang, G.; Padmanabhan, S.; Elias-Arnanz, M.; Drennan, C. L. Structural Basis for Gene Regulation by a B12-Dependent Photoreceptor. *Nature* **2015**, *526* (7574), 536–541.
(39) Rempel, S., Colucci, E., de Gier, J.W., Guskov, A., Slotboom, D. J. Cysteine-Mediated Decyanation of Vitamin B12 by the Predicted Membrane Transporter BtuM. *Nat. Commun.* **2018**, No. 2018, 1–8.
(40) Smith, S. D.; Bridou, R.; Johs, A.; Parks, J. M.; Elias, D. A.; Hurt, R. A.; Brown, S. D.; Podar, M.; Wall, J. D. Site-Directed Mutagenesis of HgcA and HgcB Reveals Amino Acid Residues Important for Mercury Methylation. *Appl. Environ. Microbiol.* **2015**, *81* (9), 3205–3217.

(41) Zhou, J.; Riccardi, D.; Beste, A.; Smith, J. C.; Parks, J. M. Mercury Methylation by HgcA: Theory Supports Carbanion Transfer to Hg(II). *Inorg. Chem.* **2014**, *53* (2), 772–777.
(42) Koay, M. S.; Antonkine, M. L.; Gärtner, W.; Lubitz, W. Modelling Low-Potential [Fe4S4] Clusters in Proteins. *Chem. Biodivers.* **2008**, *5* (8), 1571–1587.
(43) Harder, S. R.; Lu, W. P.; Feinberg, B. A.; Ragsdale, S. W. Spectroelectrochemical Studies of the Corrinoid/Iron-Sulfur Protein Involved in Acetyl Coenzyme A Synthesis by Clostridium Thermoaceticum. *Biochemistry* **1989**, *28* (23), 9080–9087.
(44) DeSilva, T. M.; Veglia, G.; Porcelli, F.; Prantner, A. M.; Opella, S. J. Selectivity in Heavy Metal-Binding to Peptides and Proteins. *Biopolymers* **2002**, *64* (4), 189–197.
(45) Barkay, T.; Miller, S. M.; Summers, A. O. Bacterial Mercury Resistance from Atoms to Ecosystems. *FEMS Microbiol. Rev.* **2003**, *27* (2–3), 355–384.
(46) Morby, A. P.; Hobman, J. L.; Brown, N. L. The Role of Cysteine Residues in the Transport of Mercuric Ions by the Tn501 MerT and MerP Mercury-resistance Proteins. *Mol. Microbiol.* **1995**, *17* (1), 25–35.
(47) Wilson, J. R.; Leang, C.; Morby, A. P.; Hobman, J. L.; Brown, N. L. MerF Is a Mercury Transport Protein: Different Structures but a Common Mechanism for Mercuric Ion Transporters? *FEBS Lett.* **2000**, *472* (1), 78–82.
(48) Pitts, K. E.; Summers, A. O. The Roles of Thiols in the Bacterial Organomercurial Lyase (MerB). *Biochemistry* **2002**, *41* (32), 10287–10296.
(49) Brown, N. L.; Ford, S. J.; Pridmore, R. D.; Fritzinger, D. C. Nucleotide Sequence of a Gene from the Pseudomonas Transposon Tn501 Encoding Mercuric Reductase. *Biochemistry* **1983**, *22* (17), 4089–4095.
(50) Watton, S. P.; Wright, J. G.; MacDonnell, F. M.; Bryson, J. W.; Sabat, M.; O'Halloran, T. V. Trigonal Mercuric Complex of an Aliphatic Thiolate: A Spectroscopic and Structural Model for the Receptor Site in the Hg(II) Biosensor MerR. *J. Am. Chem. Soc.* **1990**, *112* (7), 2824–2826.
(51) Wang, D.; Huang, S.; Liu, P.; Liu, X.; He, Y.; Chen, W.; Hu, Q.; Wei, T.; Gan, J.; Ma, J.; et al. Structural Analysis of the Hg(II)-Regulatory Protein Tn501 MerR from Pseudomonas Aeruginosa. *Sci. Rep.* **2016**, *6*, 1–9.

Chapter 2 HgcB

2.1 Introduction

Methylmercury (MeHg) is a neurotoxin synthesized by microorganisms containing the *hgcAB* genes[1]. Understanding the biosynthesis of MeHg is vital due to the risks posed to aquatic fish and bird species, as well as fish-consuming human populations, by environmental conversion of Hg(II) to MeHg[2,3]. Little is known about the biochemical mechanism by which this occurs, but it has been shown that deletion of either *hgcA* or *hgcB* eliminates the ability of *Desulfovibrio desulfuricans* ND132 and *Geobacter sulfurreducens* PCA to methylate mercury (Hg) in culture. These genes encode a 40kDa corrinoid-dependent methyltransferase with a C-terminal transmembrane domain and a 10kDa ferredoxin-like protein with two four-iron four-sulfur ([4Fe-4S]) consensus motifs, respectively. Based on similarity to characterized corrinoid-dependent methyltransferase reactions, notably methionine synthase (MetH) and the corrinoid iron-sulfur protein (CFeSP)[4], it is proposed that the HgcA corrinoid is reduced by HgcB to the Co(I) state, methylated by an as yet unidentified methyl donor, and the methyl group transferred to Hg(II), resulting in an inactive Co(III) state. HgcB has two proposed roles in this model: to supply low-potential electrons through its [4Fe-4S] clusters to reduce the HgcA corrinoid cofactor each catalytic cycle and to bind the Hg(II) substrate via its conserved cysteine (Cys) residues.

[4Fe-4S] clusters are ancient and ubiquitious cofactors known to store and transfer low potential electrons[5]. These are generally encoded by the consensus sequence CXXCXXCXXXCP and incorporate 4 atoms of divalent iron Fe and 4 equivalents of sulfide. The Fe atoms are coordinated by the Cys residues and bridged by sulfide ions, resulting in a cubane structure with an overall charge of +2 in the oxidized state. 1 electron reduction of this cofactor results in the delocalization of that electron within the cluster and a formal reduced charge of +1. Low-potential clusters have been observed with midpoint redox potentials ranging from -280mV to -705mV[5]. The Co(II) to Co(I) redox couple is low in the range of biological potentials, and reductions of MetH and CFeSP exhibit midpoint redox potentials of -526mV[6] and

-504mV[7], respectively. MetH is reduced by the higher potential flavodoxin protein, but the protein environment surrounding the corrinoid shifts the effective midpoint potential of the Co(II)/Co(I) couple by +50mV make the reduction by flavodoxin more favorable[8]. In the CFeSP, an internal [4Fe-4S] cluster is responsible for reduction of Co(II) and its 2+/1+ midpoint potential has been determined as -523mV. Thus it is hypothesized that the HgcB iron-sulfur clusters are sufficiently low in potential to reduce a similar corrinoid species.

Initial attempts by our collaborators at Oak Ridge National Laboratory to heterologously produce the *hgcB* gene from *Desulfovibrio desulfuricans* ND132 in *Escherichia coli* BL21 cells resulted in insoluble protein. Two approaches were combined to obtain soluble, iron-replete HgcB. The first was the cloning of a series of fusion protein constructs and testing their expression level and solubility after cell lysis. A maltose binding protein (MBP) tag was chosen for its high expression, solubility, and ease of purification via affinity resin. The second was the use of a co-expression plasmid shown to increase [4Fe-4S] cluster loading in overexpression systems[9]. The Ragsdale laboratory routinely uses co-expression systems in which cofactor uptake and/or assembly genes are encoded on a plasmid and co-transformed into the cell line expressing the protein of interest. The pRKISC plasmid was used in the expression of HgcB for characterization by UV-visible spectroscopy and EPR to assess its [4Fe-4S] motifs.

Another feature of interest in HgcB is its conserved Cys residues: Cys73, Cys94, and Cys95. Hg exhibits a high affinity for thiolate coordination and Hg binding proteins must compete with Hg complexation by intracellular thiolates. Peptide studies of Cys-Cys motifs have indicated both high affinity and specificity for Hg(II) over other thiophilic metals[10]. Several examples of vicinal Cys-Cys motifs are seen in the *mer* operon[11], which encodes MeHg trafficking and detoxification genes and is highly specialized to bind Hg with high affinity. Though none of the relevant Cys residues are vicinal in sequence, an unusual 3-coordinate Cys-Cys-Cys Hg(II) binding site is observed in the MerR transcriptional regulator[12], which may also bear relevance to Hg binding by HgcB. *In vivo* mutagenic studies of Cys73, Cys94, and Cys95 indicated the effect of alanine (Ala) substitution of these residues on *in vivo* Hg methylation activity in *Desulfovibrio desulfuricans* ND132[13]. These data are summarized in Table 1 and suggest that Cys73 and either Cys94 or Cys95 are required for MeHg production.

HgcB mutation	% MeHg produced
C73A	None detected
C94A	109%
C95A	120%
C94A/C95A	4%

Table 2.1 Effect of Cys substitution with Ala at Cys 73, Cys94, and Cys95 on in vivo MeHg production in Desulfovibrio desulfuricans ND132. Percent values of MeHg produced are in comparison to the wild-type strain (adapted from Ref. 11).

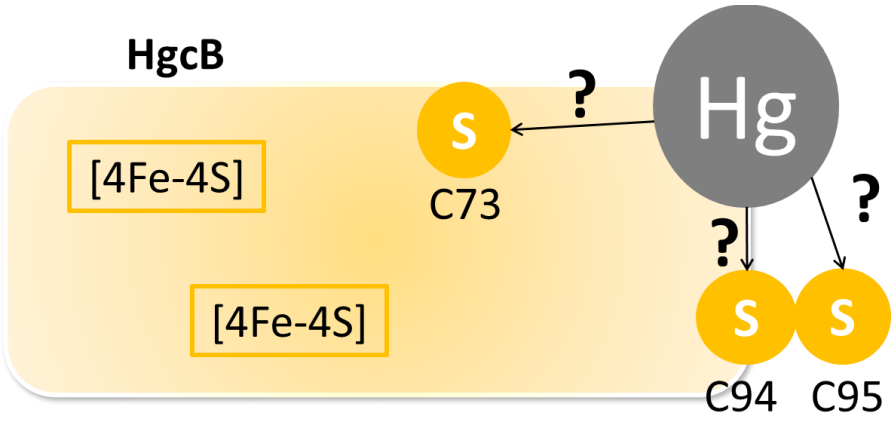

Figure 2.1 Schematic representation of the HgcB conserved cysteines. Cys94 and Cys95 are found on the C-terminus of the protein and thus likely to be exposed. The structural accessibility of Cys73 is unknown.

We hypothesize that some configuration of the HgcB conserved Cys residues comprise a high-affinity Hg binding site. To test this hypothesis, we used stopped-flow kinetics to observe the dissociation of a colorimetric ligand, 2-nitro-5-thiobenzoate (TNB), from Hg(II) upon mixing with HgcB. $Hg(TNB)_2$ is a high-affinity, stable complex, and only a high-affinity Hg binding site could rapidly induce its dissociation This mimics the proposed role of HgcB in binding intracellular Hg(II), which is typically coordinated to small molecule thiolates; we therefore view this experiment as a functional assay. We sought to test whether the same analysis of a variety of Cys73, Cys94, and Cys95 mutants would indicate deficiencies in their ability to bind Hg, suggesting which Cys residues are required for Hg binding.

2.2 Materials and Methods

2.2.1 Materials

All chemicals were purchased from Sigma-Aldrich (St. Louis, MO) unless otherwise stated. All custom synthesized oligonucleotide primers were ordered from Integrated DNA Technologies (Coralville, Iowa). All restriction enzymes, the Q5 Site-directed mutagenesis kit, and amylose resin were purchased from New England Biolabs (Ipswich, MA). Pfu Ultra polymerase was used for all PCR reactions and obtained from Agilent (Santa Clara, CA). BL21(DE3) and TOP10 chemically competent cell lines were obtained from Invitrogen/Life Technologies (Carlsbad, CA). P2 resin was purchased from Bio-Rad (Hercules, CA). The codon-optimized HgcB plasmid was custom synthesized by DNA2.0 and provided to us as a gift from Dr. Alexander Johs, Oak Ridge National Laboratory. cOmplete EDTA-free protease inhibitor tablets were acquired from Roche (Indianapolis, IN). Titanium (III) citrate was prepared similarly to the method of Zehnder and Wurhmann[14] in 1M Tris-HCl pH 8.0. Maltose binding protein (MBP) was purified and provided by Dr. Eric Carter.

2.2.2 HgcB fusion tag screen

Ligation independent cloning was used to generate a series of HgcB constructs with the N-terminal fusion protein tags GB1[15], MBP[16], Mocr[17], and SC-Mocr. The destination vectors are all derived from the pMCSG7 system and include an N-terminal His_6 tag, the fusion protein tag, and a TEV proteolysis sequence upstream of the protein of interest[18]. Vectors were transformed into TOP10 cells and plated on LB agar selection plates containing 100ug/mL ampicillin. Sequences were verified by Sanger sequencing using the T7 terminator primer (University of Michigan DNA Sequencing Core) and transformed into BL21(DE3) cells. Cultures grown from single colonies were stored at -80°C in 25% glycerol and used to inoculate overnight starter cultures.

To test the expression of each of the four HgcB fusion constructs in BL21(DE3) cells, LB overnight cultures containing 100ug/mL ampicillin were inoculated from frozen cell stocks. 1mL of each overnight culture was used to inoculate 1L of LB media containing 100ug/mL ampicillin and incubated at 37°C with 225rpm shaking. Expression was induced by addition of 1mM IPTG between OD_{600} 0.6-0.7. After 3 hours, the cells were harvested by centrifugation and frozen at -

20°C. Whole-cell gel samples were taken before and after induction and analyzed by nonreducing SDS-PAGE on a 12% polyacrylamide gel.

Each cell pellet was resuspended in 10mL MOPS pH 7, 100mM NaCl, and 5mM DTT and sonicated at 4°C. 100uL of the lysis mixture was aliquoted into a microcentrifuge tube and centrifuged at 17,000xg in a tabletop microcentrifuge. The soluble lysate was removed and added to 100uL of 2X LDS sample loading buffer and 200uL 1X LDS buffer was used to resuspend the insoluble pellet fraction. These samples were analyzed by nonreducing SDS-PAGE on a 12% polyacrylamide gel to determine the solubility of each construct after lysis.

2.2.3 MHB co-expression with pRKISC and affinity purification

The protocol for overexpression of MBP-HgcB was modified from existing procedures for the heterologous expression of Fe-S proteins[19,20]. The vector containing His_6-MBP-HgcB, abbreviated hereafter as MHB, was co-transformed into BL21(DE3) cells with the pRKISC vector and plated on LB agar selection plates containing 100ug/mL ampicillin and 5ug/mL (50% working concentration) tetracycline. A glycerol stock was prepared from a single resulting colony and used to inoculate LB overnight starter cultures. 20mL of an overnight culture containing LB medium, 100ug/mL ampicillin, and 10ug/mL tetracycline was used to inoculate 1L of TB medium in a 1L bottle containing the same antibiotic concentrations. This was incubated at 37°C with 125rpm shaking until an OD_{600} ~0.6 was reached. At this point, each bottle was sealed with a septum and screw-cap ring and sparged with nitrogen gas for 1 hour. An additional 50ug/mL ampicillin and a reducing solution of 1mM sodium sulfide nonahydrate and 1.5mM L-cysteine were added to each culture via syringe and incubated for 10 minutes. 0.5mM ferrous ammonium sulfate was added and 0.5mM IPTG was used to induce expression of the *isc* genes and MHB. Cultures were incubated overnight (18-20hrs) at 15°C with 125rpm shaking. Cells were harvested by centrifugation and stored at -20°C.

Cell lysis and amylose affinity purification were conducted under anoxic conditions (< 1ppm oxygen) in a Vacuum Atmospheres anaerobic glove box. A cell pellet obtained from 4L of culture (~12g) was thawed in 50mL of lysis buffer containing 25mM Na HEPES pH 7.5, 5mM DTT, and 1 cOmplete EDTA-free protease inhibitor with gentle stirring. Cells were sonicated and the lysate cleared by centrifugation at 100,000xg. The soluble lysate was immediately applied to an amylose affinity column equilibrated with 5 column volumes (CV) of 25mM Na

HEPES pH 7.5 and 5mM DTT. 2.5CV of this buffer was used to wash the column and MHB was eluted with the same buffer containing 20mM maltose. The purified protein was analyzed for purity by sodium dodecyl sulfate polyacrylamide gel electrophoresis (SDS-PAGE) and the protein concentration determined by Bradford assay[21]. Purified MHB was stored in an anaerobic chamber at 4°C.

2.2.4 Construction of MHB cysteine mutants by site-directed mutagenesis

C94A, C95A, and C94A/C95A mutants were constructed using the QuikChange II site-directed mutagenesis protocol (Agilent) and transformed into TOP10 chemically competent cells. Successful transformants were chosen as single colonies from LB agar selection plates containing 100ug/mL ampicillin and verified by Sanger sequencing using the T7 terminator primer (University of Michigan DNA Sequencing Core). Cys73 mutants were constructed using the Q5 site-directed mutagenesis kit, transformed into NEB 5-alpha cells, and verified by Sanger sequencing as above. The MHB-CCC, MHB-CAC, MHB-CCA, or MHB-CAA vectors previously assembled were used as templates for the Cys73 mutagenesis reactions, resulting in the list of MHB variants below (Table 2). All expression of MHB Cys variants was conducted as described in section 2.2.3.

Identifier	**Mutations**
MHB-CCC	none
MHB-CAC	C94A
MHB-CCA	C95A
MHB-CAA	C94A/C95A
MHB-SCC	C73S
MHB-SAC	C73S, C94A
MHB-SCA	C73S, C95A
MHB-SAA	C73S, C94A, C95A

Table 2.2 List MHB Cys variant identifiers used in this work

2.2.5 UV-visible spectroscopy and reductive titrations of MHB

Purified MHB was exchanged into 20mM potassium phosphate (KPi) pH 7.4 using a 30kDa MWCO centrifugal concentrator. The UV-visible spectrum was measured using an Agilent/HP 8453 UV-visible spectrophotometer in a quartz cuvette. A solution of the same buffer was used as a baseline spectrum. Sequential additions of titanium (III) citrate were used to generate a reduced MHB spectrum until the 390nm – 420nm region of the spectrum was no

longer quenched by further addition of reductant. The reduced spectrum was subtracted from the oxidized spectrum to generate a difference (Δ) spectrum, from which the [4Fe-4S] cluster concentration could be calculated using established molar extinction coefficients (Abs390 = 4mM-1 iron and Δ415 = 8.2mM-1 for a protein containing two [4Fe-4S] clusters)[22]. All MHB variants were titrated with Ti citrate in the same manner.

2.2.6 EPR spectroscopy of MHB

A MHB EPR sample was prepared by buffer exchange into 20mM KPi pH 7.4 and concentration to 250uM (500uM [4Fe-4S]). 10 equivalents (5mM) of titanium (III) citrate were added to the concentrated protein solution and allowed to incubate for 1 hour. Unreacted titanium (III) citrate was removed by buffer exchange in a centrifugal concentrator. The sample was transferred to an EPR tube and frozen in liquid nitrogen. X-band EPR data were collected at 8.6K in a Bruker EMX spectrometer. The EPR instrument is equipped with a Bruker/ColdEdge helium cryostat and recirculation system and an Oxford Instruments Mercury iTC temperature and gas flow controller.

2.2.6 $Hg(TNB)_2$ complex preparation and MHB titration

The $Hg(TNB)_2$ complex was prepared from DTNB and mercuric acetate according to published methods[23] and purified by isocratic gel filtration into 50mM KPi pH 7.4 using a P2 column. Fractions were assessed in the UV-visible range for the presence of a single peak at 354nm and frozen at -20°C until use. $Hg(TNB)_2$ concentration was determined using the extinction coefficient of $20.8mM^{-1}$ at 354nm. The MHB and MBP to be titrated with $Hg(TNB)_2$ were exchanged into 20mM KPi 7.4 by centrifugal ultrafiltration using a 30kDa MWCO. The protein samples were prepared in a Vacuum Atmospheres anaerobic glove box in quartz cuvettes and sealed with rubber stoppers. UV-visible measurements were conducted with a Shimadzu UV-2600 spectrophotometer outside of the anaerobic environment, and $Hg(TNB)_2$ addition to the sample was made via gas-tight Hamilton syringe through the rubber septum.

2.2.7 Stopped-flow kinetic studies of MHB variants and $Hg(TNB)_2$

MHB samples for stopped flow experiments were prepared anaerobically by buffer exchange into 20mM KPi pH 7.4. The concentration of all protein samples were adjusted to 25uM, as indicated by a 390nm absorbance of ~0.8. $Hg(TNB)_2$ as prepared in section 2.2.6 was

diluted to 25uM in the same buffer. This buffer was also used to collect a baseline spectrum prior to stopped-flow data collection. Rapid kinetic analysis of the MHB-Hg binding interaction was conducted using an Applied Photophysics stopped-flow instrument housed in a Vacuum Atmospheres anaerobic glove box with an atmospheric oxygen concentration < 1ppm O_2. All data were collected for 1 second at 20°C in photodiode array (PDA) mode using the 1cm path length configuration of the instrument. Stopped flow traces were collected in triplicate and fit to a double exponential model using ProData Viewer software. The deadtime of our instrument has been characterized as 1.8ms[24], so data were fit from 2ms-1s. The MHB-SCC variant was the exception to this data treatment and could only be fit to a single exponential model. Standard deviations of triplicate observed rate constant values and amplitude values from the kinetic curve fits were calculated and plotted as error bars.

2.3 Results and Analysis

2.3.1 SDS-PAGE analysis of HgcB fusion tag screen

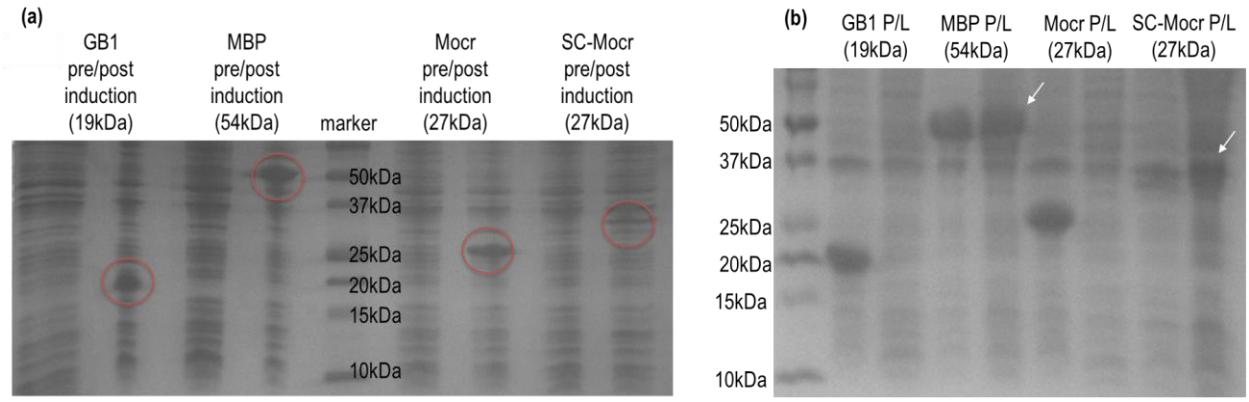

Figure 2.2 SDS-PAGE analysis of HgcB fusion tag screen (a) Nonreducing SDS-PAGE analysis of whole-cell samples collected during test expressions of HgcB fusion constructs. Each set of samples is labelled by N-terminal tag and the left and right lanes represent samples collected immediately prior to IPTG induction and samples collected after 3 hour induction, respectively. (b) Nonreducing SDS-PAGE analysis of insoluble pellet and soluble lysate fractions after lysis of cells containing each of the four HgcB constructs. Samples are labelled as in (a) and lanes correspond to the pellet (P) and lysate (L) fractions, respectively.

Expression of HgcB variants after IPTG induction was indicated by the appearance of a gel band near the calculated MW of each fusion tagged construct. These are circled in red in Figure 2.2a and are not present in the pre-induction samples. After cell lysis, the distribution of

each construct in the insoluble (P) and soluble (L) fractions is shown in Figure 2.2b and indicated by arrows. From this it can be concluded that GB1-HgcB and Mocr-HgcB are not soluble after cell lysis under these conditions, and this gel is inconclusive in determining the fractionation of SC-Mocr-HgcB. MBP-HgcB is soluble after cell lysis, though some remains in the insoluble fraction.

2.3.2 MHB expression and amylose affinity purification

In a typical MHB preparation, ~2-3g of cells (wet weight) were obtained per L of culture. Due to iron precipitates observed in the harvested cells, a reliable final OD measurement could not be obtained. Brown colored fractions eluted from amylose affinity resin were collected and analyzed by SDS-PAGE. The gel revealed a band around the 50kDa molecular weight marker which we identify as MHB (54kDa) and a band below it around 45kDa (Figure 2.3, lane 2). This is consistent with the molecular weight of the MBP protein, and Western Blot analysis revealed that this band did bind an anti-MBP antibody (data not shown). A typical MHB preparation yielded approximately 25 mg of MHB as determined by Bradford assay. The MHB variants listed in Table 2.2 were expressed and purified as above with comparable cell density and purified protein yields. In Figure 2.3, SDS-PAGE analysis of purified MHB variants showed that the purified Cys mutants also exhibit this double banding pattern by SDS-PAGE, though the relative intensities of the two bands varies between preparations.

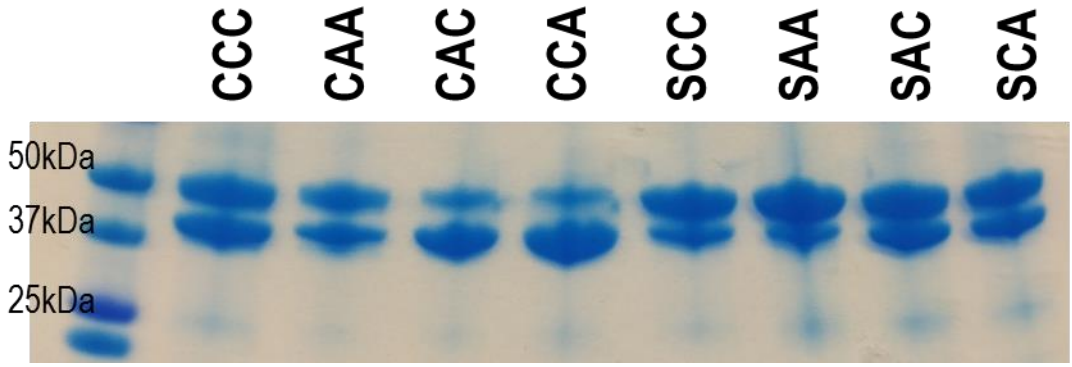

Figure 2.3 SDS-PAGE analysis of purified MHB variants. Amylose affinity column elution of each MHB variant. Lanes are labelled according to the Cys variant identifiers listed in Table 2.2.

2.3.3 UV-visible spectroscopy and reductive titration of MHB variants

Reduction of MHB and variants with titanium (III) citrate was monitored by observing the characteristic decrease in absorbance intensity in the 390nm-420nm region seen in many [4Fe-4S] proteins[25], and is shown in Fig 2.4 below. Sequential additions of titanium (III) citrate were made until the 415nm absorbance reached a minimum; this required 3-4 equivalents titanium (III) citrate for all variants. A characteristic reductive titration of the MHB-CCC variant is shown in Figure 2.4.

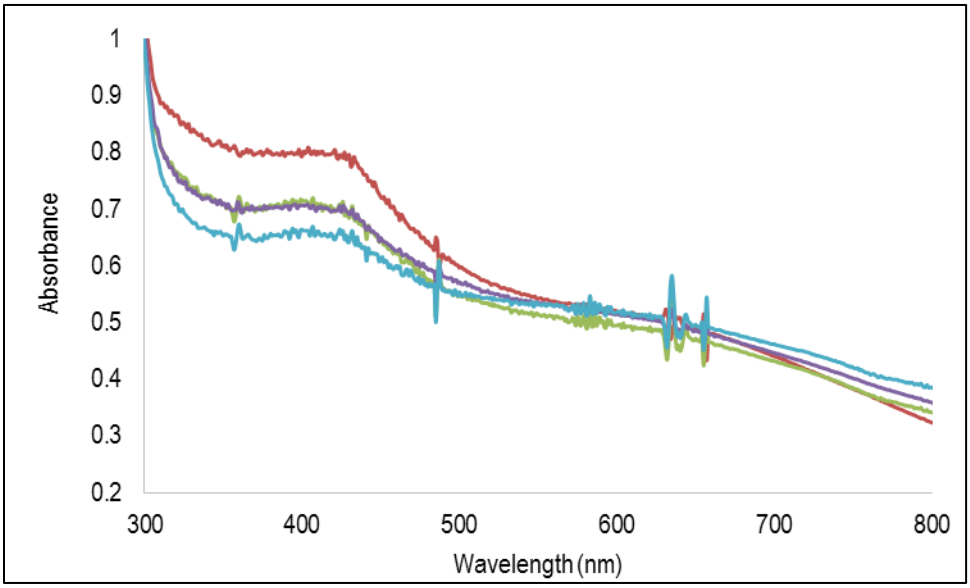

Figure 2.4 Titanium (III) citrate reduction of MHB-CCC. 25uM MHB-CCC was titrated with titanium (III) citrate by sequential additions of 25uM (1 equivalent). These data are representative of similar titrations of MHB variants with titanium (III) citrate.

As ferredoxins are typically small proteins, the ratio between the 280nm and 390nm absorbance can generally be used to determine the iron occupancy with good accuracy[25]. The 280nm aborbance value of MHB, however, is saturated by contributions from the MBP fusion protein. The iron occupancy of [4Fe-4S] clusters can also be estimated by using the molar extinction coefficient at of $4mM^{-1}$ Fe atoms at 390nm[25]; these values are calculated in the center columns of Table 2.3. If the value of Δ415nm is used to calculate protein concentration based on the value of ε(Δ415nm) = 8.2mM-1 for a protein containing two [4Fe-4S] clusters[22], the MHB concentration values in the leftmost columns of Table 2.3 are in relatively good agreement with those determined from the 390nm absorbance. Cluster occupancy was calculated by comparing

the [MHB] derived from the Δ415nm absorbance values obtained after Ti citrate reduction to the protein concentration determined by Bradford assay.

variant	Δ415nm	[cluster] (uM)	[MHB] (uM)	Abs390	[Fe] (uM)	[MHB] (uM)	[MHB] by Bradford assay (uM)	cluster occupancy
CCC	0.1519	37.0	18.5	0.7979	199.5	24.9	11.4	**163%**
CAA	0.1595	38.9	19.5	0.8133	203.3	25.4	15.3	**127%**
CAC	0.0979	23.9	11.9	0.7861	196.5	24.6	20.7	**58%**
CCA	0.2034	49.6	24.8	0.8091	202.3	25.3	22.4	**111%**
SCC	0.2061	50.3	25.1	0.8234	205.9	25.7	22.2	**113%**
SAA	0.1992	48.6	24.3	0.8514	212.9	26.6	18.6	**131%**
SAC	0.1682	41.0	20.5	0.8123	203.1	25.4	23.7	**86%**
SCA	0.2373	57.9	28.9	0.8333	208.3	26.0	17.0	**170%**

Table 2.3 UV-visible absorbance features of MHB variants and cluster occupancy calculation. Three methods of MHB concentration determination are shown from left to right: calculation of the concentration of titratable [4Fe-4S] cluster at 415nm, correlation of the 390nm absorbance value to Fe atom concentration, and comparison to a protein standard curve by Bradford assay.

The cluster occupancy values in Table 2.3 were surprising when associated with the SDS-PAGE analysis in Figure 2.3. If the upper band of each gel lane corresponds to the fusion protein, it would be expected that approximately 25%-50% of the total protein concentration, as determined by Bradford assay, would correspond to MHB. In light of these results, we conclude either (a) the Bradford assay does not reliably represent the concentration of MHB or (b) the lower molecular weight gel band is also MHB, possibly a truncated product, and contains the MHB [4Fe-4S] clusters. For the purposes of concentration determination and consistency, the absorbance at 390nm was used to standardize the concentration of MHB across MHB variants in further experiments.

2.3.4 MHB-CCC EPR spectrum

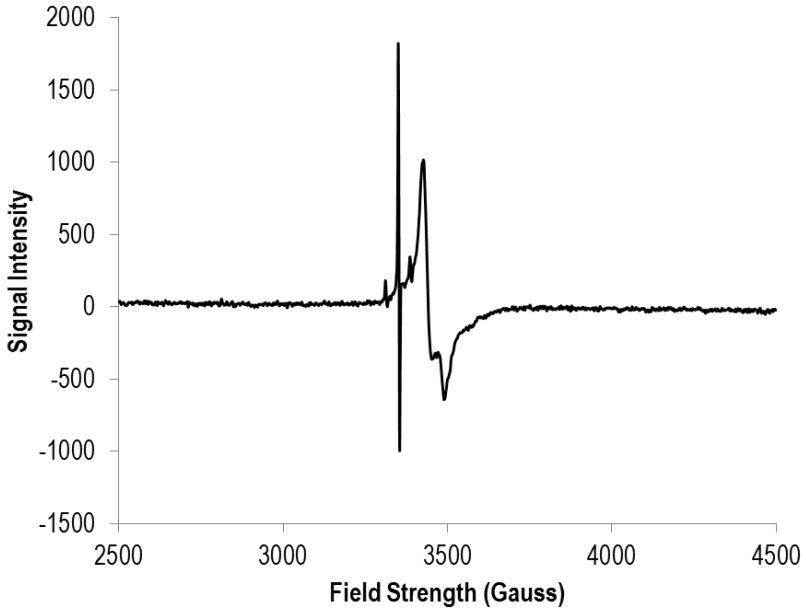

Figure 2.5 EPR spectrum of MHB-CCC prepared by reduction with titanium (III) citrate Data collection parameters: 1mW power, 5G amplitude modulation, $4.5x10^3$ gain, and 9.38 GHz frequency at 8.6K.

No EPR spectrum was detected in samples prepared by reduction with excess sodium dithionite (Em ~ -444mV vs. NHE); this may suggest that the MHB [4Fe-4S] clusters are quite low in potential and require a stronger chemical reductant, such as titanium (III) citrate (Em ~ -550mV vs. NHE)[26]. The EPR spectrum of MHB-CCC was obtained after incubation with 10 equivalents of titanium (III) and removal of excess reductant by buffer exchange. The spectrum collected at 8.6K can be seen in Figure and exhibits the characteristic feature of [4Fe-4S] clusters centered at g = 1.94[27]. Another signal centered at g = 2.0 is observed which bears resemblance to an organic radical species – this can be observed as an artifact of EPR cavity contamination and we hesitate to assign this feature to MHB.

2.3.5 $Hg(TNB)_2$ titration of MHB-CCC

Addition of Hg(II) species to iron-sulfur proteins is an established method for disruption of iron-sulfur clusters[28] and inorganic Hg(II) exposure in *Escherichia coli* induces a rapid increase in intracellular labile iron, thought to occur due to disruption of protein-associated iron-sulfur clusters[29]. As we are interested in testing the hypothesis that the 3 MHB conserved Cys

residues are involved in Hg(II) binding, we sought to minimize the potential for Hg to bind adventitiously to the 8 Cys residues involved in the [4Fe-4S] cluster motifs. 2-nitro-5-thiobenzoate (TNB^-), the disulfide of which is known as Ellman's reagent[30], forms a stable complex with Hg(II) and has been used by Ledwidge et.al. to supply Hg(II) to proteins containing high-affinity Hg binding sites[23]. As discussed in this work, the authors reasoned that both the TNB- ion and a protein Cys thiolate are high-affinity ligands for Hg(II), but the lower pKa of TNB should be more favored than anything other than coordination by an available Cys thiolate. We synthesized $Hg(TNB)_2$ according to published methods and titrated it against MHB-CCC. The $Hg(TNB)_2$ complex exhibits a UV-visible maximum at 354nm, whereas the TNB anion peak is centered at 408nm. This provides for facile colorimetric observation of TNB anion release as an indirect measure of Hg(II) binding to the protein.

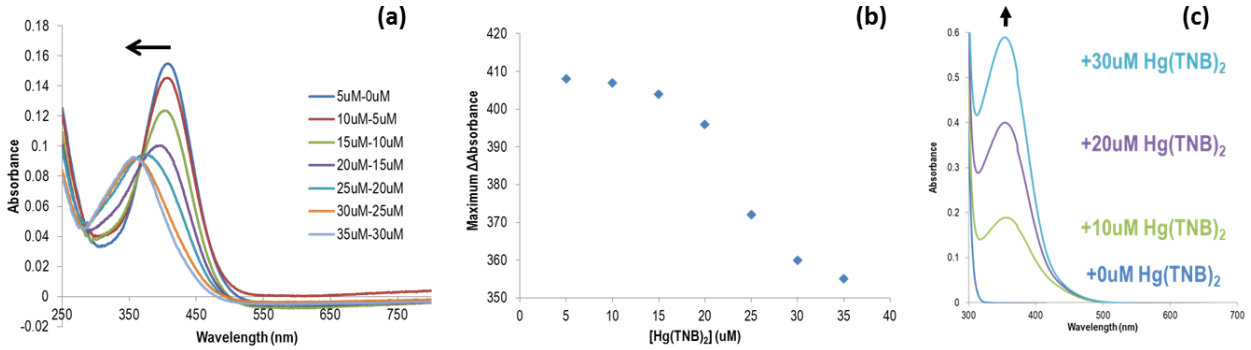

Figure 2.6 $Hg(TNB)_2$ titrations of 6uM MHB-CCC and 20uM MBP (a) Difference spectra obtained between sequential additions of 5uM increments of $Hg(TNB)_2$ to 5uM MHB-CCC. (b) Wavelength maximum of the difference spectra obtained in a as a function of total $Hg(TNB)_2$ added. (c) $Hg(TNB)_2$ addition to 20uM maltose binding protein.

We determined by this method that a large excess of $Hg(TNB)_2$ dissociates upon addition of MHB-CCC (Figure 2.6a). The absorbance values at 408nm in the first three additions of $Hg(TNB)_2$ (15uM total) correspond to a total concentration of TNB^- release of 30uM, consistent with 2 equivalents per Hg(II). Further additions of $Hg(TNB)_2$ yielded a mixture of $Hg(TNB)_2$ and TNB^- peaks, and the difference spectrum ceased reflecting $Hg(TNB)_2$ dissociation after the addition of 6 equivalents of $Hg(TNB)_2$ (Figure 2.6b). Purified MBP was titrated with $Hg(TNB)_2$ to exclude the possibility that this observation was an artifact of the MBP fusion tag (Figure 2.6c). As expected, no dissociation of $Hg(TNB)_2$ was observed upon addition to MBP, which does not contain any Cys residues. The free thiol concentration of MHB-CCC was determined by reaction with Ellman's reagent as 12.7uM, which is consistent with the protein concentration of

5uM determined from the [4Fe-4S] cluster absorbance at 390nm. We suggest that the magnitude of TNB anion release presented here could be explained by the binding of Hg(II) to the MHB cluster Cys residues and concommittent disruption of the [4Fe-4S] clusters.

2.3.6 Stopped-flow kinetic analysis of Hg binding to MHB variants

Stopped-flow rapid kinetic analysis was used to compare the $Hg(TNB)_2$ dissociation rates and TNB^- release rates of a panel of MHB Cys mutants to determine if differential rates were observed between the different MHB variants. We hypothesized that Hg(II) binding to an exposed Cys binding site would occur faster than iron-sulfur cluster displacement and these two processes could be identified using this technique. The MHB variants in which Cys residues required for Hg(II) binding are substituted with Ala or Ser would presumably only exhibit the comparatively slow displacement of the MHB [4Fe-4S] clusters. Data were collected for 1 second upon mixing of 25uM $Hg(TNB)_2$ and 25uM of each MHB variant. Figure 2.7a shows a representative stopped-flow data set in which the $Hg(TNB)_2$ peak at 354nm disappears with the evolution of the TNB anion peak at 408nm and panel b overlays the absorbance values at these wavelengths over a 1 second time scale. These traces fit well to a double exponential kinetic model and these fits are overlaid with representative traces in Figure 2.7c. The exception to this data treatment is the MHB-SCC variant, in which the 408nm traces were better fit to a single exponential kinetic model (though the 354nm trace was still fit to a double exponential), shown in Figure 2.7d.

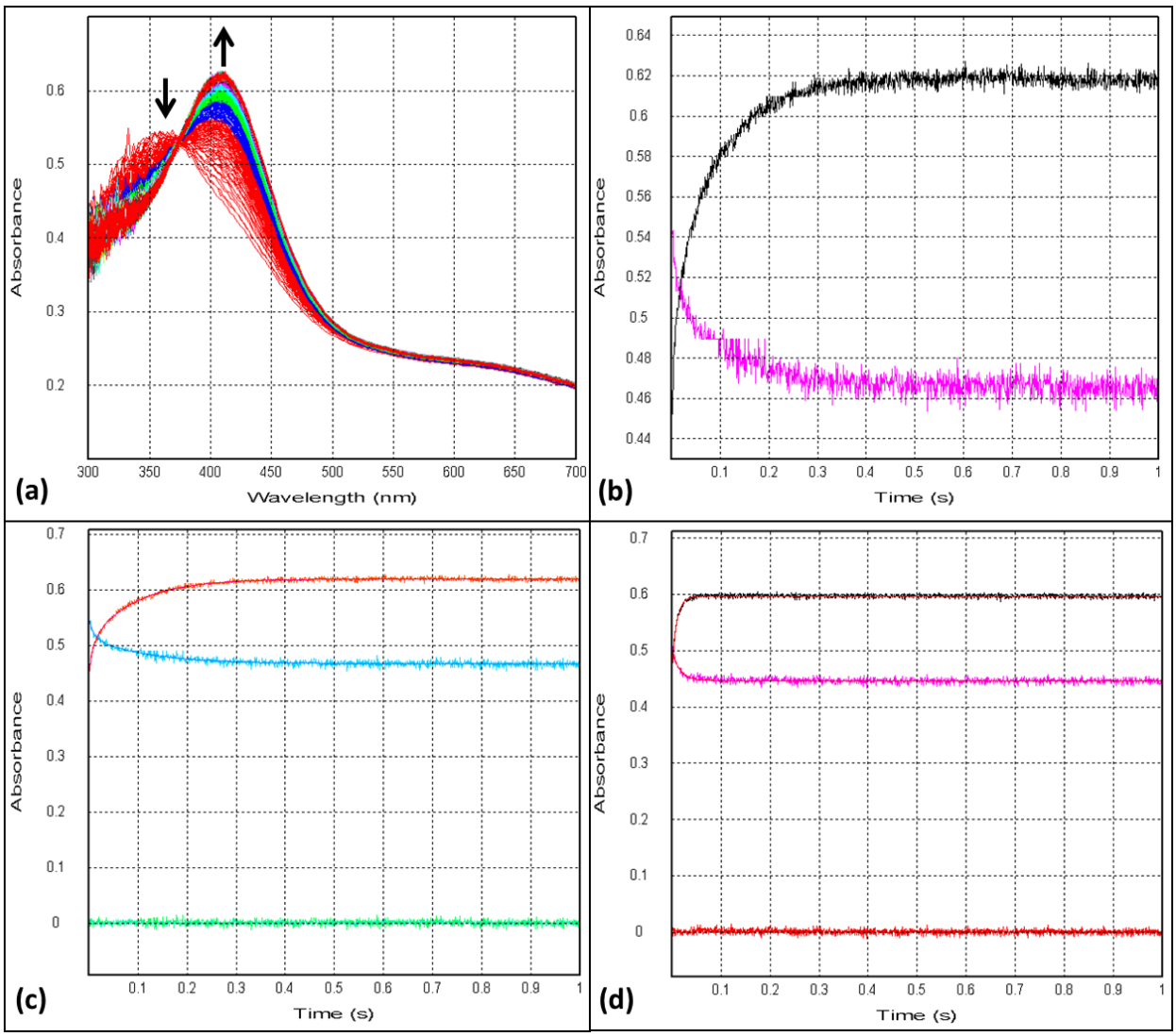

Figure 2.7 Representative stopped-flow absorbance data. (a) Overlay of spectra collected for 1s upon mixing of 25uM Hg(TNB)2 to 25uM MHB-CCC. Arrows indicate the associated decrease in 354nm absorbance and increase at 408nm. (b) Absorbance vs. time traces at 354nm (bottom, pink) and 408nm (top, black). (c) Representative double exponential curve fits overlaid with the corresponding data at 354nm and 408nm. Residuals are plotted across the bottom in green. (d) Representative single exponential curve fits overlaid with the corresponding MHB-SCC data at 354nm and 408nm. Residuals are plotted across the bottom in red.

To our surprise, all eight Cys variants induced rapid dissociation of the $Hg(TNB)_2$ complex. The observed rate constants and the corresponding absorbance amplitudes for each exponential phase are organized by wavelength, with 354nm analysis shown in Figure 2.8 and 408nm analysis in Figure 2.9. Several striking observations can be made from comparisons between these MHB variants:

(1) The rapid dissociation of $Hg(TNB)_2$ (Figure 2.8a), as indicated by the disappearance of the 354nm peak, displays rate constants of ~$100s^{-1}$ in the CCC, CAC, CCA, and SCC variants. This rate is lowered by a factor of 2 in the remaining 4 variants. The trend observed here is a *more rapid dissociation of $Hg(TNB)_2$ in variants containing two of the three relevant Cys residues*. We propose that this is consistent with a preferential binding to these residues.

(2) The TNB^- release observed in the 408nm traces of the MHB SCC variant was best fit to a single exponential model, in contrast to all other data sets (Figure 2.9). The 354nm double exponential fits for the SCC variant reveal that the absorbance change associated with the second observed rate constant phase is a small fraction of the total Δ354nm (approx. 5%, Figure 2.8b & d), indicating that the 354nm data is effectively monophasic as well. We conclude from this observation that *the MHB-SCC variant displays the simplest Hg(II) binding model in this data set*, in which $Hg(TNB)_2$ dissociation occurs at same rate (~$100s^{-1}$) of TNB^- release, indicative of Hg(II) binding to MHB-SCC at a 1:1 ratio and releasing both equivalents of TNB^-. We are unsure why this phenomenon is not also observed in the wild-type CCC variant.

(3) If some configuration of Cys73, Cys94, and/or Cys95 comprises a Hg(II) binding site, we would expect the MHB-SAA variant to be deficient in Hg(II) binding and attribute $Hg(TNB)_2$ dissociation induced by mixing with the SAA variant to the adventitious binding of Hg(II) to the [4Fe-4S] cluster Cys residues. The SAA variant appears kinetically equivalent to the CAA variant in these experiments, and both induce $Hg(TNB)_2$ dissociation at a two-fold slower rate compared to the CCC, CAC, CCA, and SCC variants containing 2 of the 3 relevant Cys residues (Figure 2.8a). This leads us to the conclusion that *wild-type Hg(II) binding requires Cys94 and/or Cys95*.

(4) The total absorbance change at both wavelengths is equivalent between all variants, but the *observed rate constants for the fast and slow phases are not consistent between the processes observed at 354nm and 408nm.* For instance, almost all $Hg(TNB)_2$ dissociation upon mixing with the MHB-CAA variant occurs primarily in the faster observed phase with a rate constant of $50s^{-1}$ (Figure 2.8a & b). 60% of the total TNB^- anion release, occurs in the slower phase observed in the data collected at 408nm, corresponding to a rate constant of $40s^{-1}$(Figure 2.9c & d). When the concentrations of these species are

calculated from these absorbance changes using their molar extinction coefficients, there is good agreement between the 3uM $Hg(TNB)_2$ consumed in this phase and 7uM TNB^- generated. We are unsure, however, of how to assign the more rapid generation of TNB^- at a rate constant of $250s^{-1}$ associated with a smaller fraction of $Hg(TNB)_2$ dissociation.

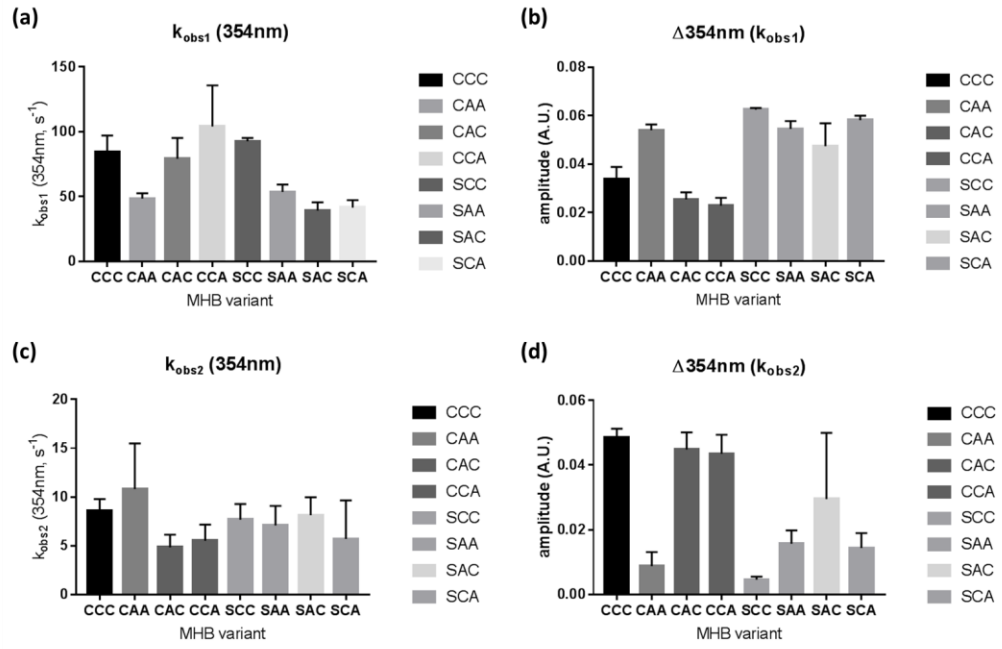

Figure 2.8 Kinetic parameters of 354nm curve fits (a) and (c) show the observed rate constants for fast (kobs1) and slow (kobs2) exponential phases in the double exponential fit, respectively. (b) and (d) show the corresponding 354nm absorbance change (amplitude) represented by each phase.

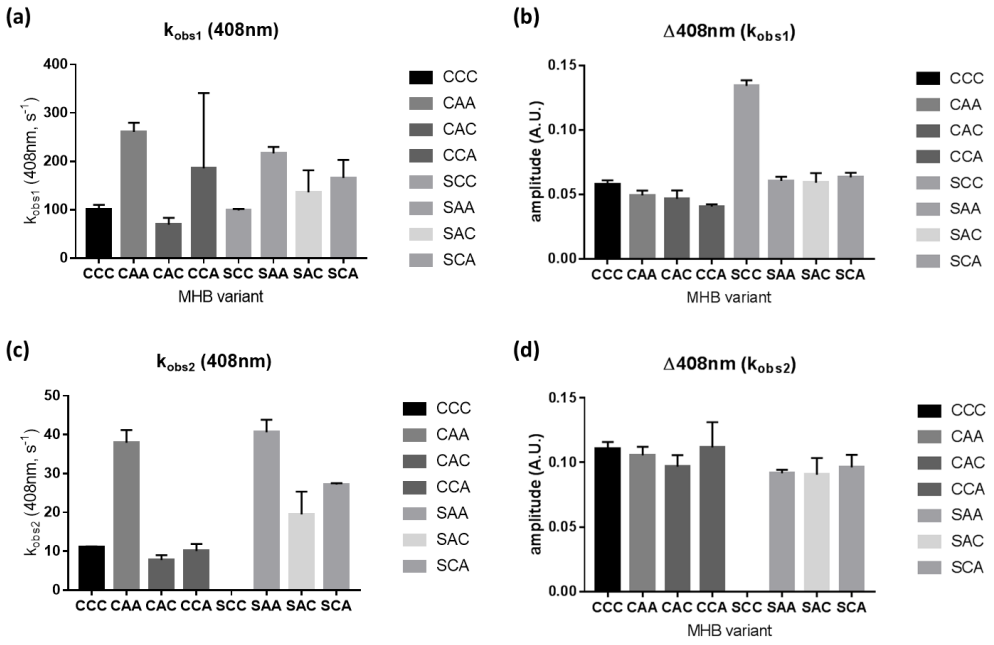

Figure 2.9 Kinetic parameters of 408nm curve fits (a) and (c) show the observed rate constants for fast (kobs1) and slow (kobs2) exponential phases in the double exponential fit, respectively. (b) and (d) show the corresponding 408nm absorbance change (amplitude) represented by each phase.

2.4 Discussion

2.4.1 Purification of MHB and Cys variants generates an iron-replete [4Fe-4S] protein

MBP was found to have a positive effect on HgcB expression as a solubilizing affinity fusion tag and the resulting fusion protein, abbreviated MHB, was expressed with the pRKISC co-expression system resulting in the purification of iron-replete protein. Expression and purification of seven MHB variants yielded similar results. Figure 2.3 shows the presence of two bands in SDS-PAGE analysis of all MHB variants, the ratio of which varies between protein preparations. The higher molecular weight band is consistent with the weight of the MHB fusion protein (54kDa) and the lower is consistent with the weight of MBP (43kDa). Both bands were found to react with a polyclonal MBP antibody (data not shown) and we are unsure whether the lower band represents MBP not associated with HgcB or a truncated MHB product which retains the [4Fe-4S] clusters. This complicates the determination of protein concentration by Bradford assay, so concentrations are instead standardized to the UV-visible features of the [4Fe-4S] clusters.

The UV-visible spectra of all MHB variants were similar and used to observe the reduction of the [4Fe-4S] clusters by titanium (III) citrate. It was found that sodium dithionite was unable to reduce MHB and 3-4 equivalents of Ti citrate were required to fully reduce both [4Fe-4S] clusters. The requirement for excess titanium (III) citrate, which has a reported midpoint redox potential of -550mV at pH 7, as well as the lack of complete reduction observed in the presence of dithionite may indicate that the average potential of the MHB [4Fe-4S] clusters may be quite low. The EPR spectrum of MHB-CCC is presented in Figure 2.5 and exhibits the characteristic S = ½ axial feature of [4Fe-4S] clusters centered at g = 1.94[27]. We are currently not assigning the g = 2.0 feature to the MHB protein and working to determine whether this signal is caused by organic radical contamination. Overall, MHB appears to exhibit standard characteristics of ferredoxin-like proteins containing 2 [4Fe-4S] motifs.

2.4.2 $Hg(TNB)_2$ addition to MHB results in superstoichiometric release of TNB^-

A colorimetric $Hg(TNB)_2$ complex was used to titrate MHB and probe its Hg(II) binding characteristics. This complex was used because the affinity of Hg(II) for TNB^- complexation should only be bested by Cys thiolate coordination at neutral pH based on their relative pKa values[23], so its colorimetric dissociation should indicate the stoichiometry of Hg(II) binding to MHB. This experiment indicated a release of TNB^- far in excess of the protein concentration – this is not unsurprising considering that MHB contains 11 Cys residues and Hg(II) addition has long been used to disrupt iron-sulfur clusters[28,31]. These data, in the context of relative binding affinities between MHB mutants lacking different combinations of the Cys73/Cys94/Cys95 residues implicated in *in vivo* functionality[13], indicate that titration of a triple mutant lacking all three cysteines will still likely induce TNB^- release, as it still contains 8 Cys residues involved in the [4Fe-4S] cluster motifs. This result presented a challenge to determination of the Hg(II) binding characteristics of MHB. Our goals were to (a) determine the Hg binding stoichiometry of HgcB and (b) identify the Cys residues required for retain that stoichiometry, but the indirect quantification of Hg(II) transfer by TNB^- release proved too ambiguous to determine this.

2.4.3 Stopped-flow kinetic comparison between Hg(II) binding rates of MHB variants is consistent with observed *in vivo* requirements for conserved Cys residues

We then turned to stopped-flow experiments with the hypothesis that Hg(II) binding to the predicted Hg binding site would occur rapidly, whereas disruption of the protein [4Fe-4S] clusters would indicate a slower observed rate constant. We hypothesized that the Hg binding stoichiometry could be calculated from the amplitude of the predicted fast phase, and the eventual disruption of the [4Fe-4S] clusters could be deconvoluted from the Hg binding event, allowing side-by-side comparison of MHB variants with varying configurations of Cys residues. The stopped-flow data obtained by stoichiometric mixing of $Hg(TNB)_2$ and 8 MHB Cys variants did not indicate such a straightforward assignation of kinetic phases.

Hg(II) has a strong preference for linear thiolate coordination environments, and its ligand exchange reactions have been shown to occur via transient 3-coordinate thiolate complexes rather than through initial dissociation of one of the two thiolate ligands[32]. We suggest this explains the observation that MHB variants containing at least two of the conserved Cys residues (CCC, CAC, CCA, and SCC) exhibit the fastest rates (~$100s^{-1}$ in both the 354nm and 408nm fits) of $Hg(TNB)_2$ decomposition, consistent with the rapid, sequential displacement of both TNB- ligands by MHB Cys residues. In the SCC variant, this was the only phase observed and the rate constant was equivalent to the observed rate of TNB^- release, indicating a simple stoichiometric binding interaction. Vicinal CC motifs are known to select for Hg(II) with high affinity and preference over other thiophilic metal ions, so this is unsurprising[10]; the unusual result by comparison is that the observed rate constants for the CCC construct do not follow the same trends.

The CCC (wild-type) MHB construct displays two phases in its decay of $Hg(TNB)_2$, of which the slower phase comprises ~60% of the total Δ354nm (Figure 2.8). Taken with the simple binding of Hg(II) to the SCC variant, this seems to indicate that Hg(II) binds quickly and rapidly to the C-terminal Cys residues, but some other process follows in the case of the CCC mutant. We are unsure what this process may be. The mercuric ion reductase, MerA, binds Hg(II) via a series of Cys residues to ultimately deliver it to the enzyme catalytic site for reduction by NADPH[11]. Intermediate steps in this process rely on the presence of an exogenous thiolate ligand to the Hg(II) to prevent the formation of an inactive complex between two nearby Cys residues[33].

It is possible that Cys73 is the ultimate destination of the Hg(II) ion but it is first bound by the C-terminal Cys residues 94 and 95. The transfer of Hg(II) from Cys94/Cys95 to Cys73 could drive an equilibrium in which the Hg(II) is not stably bound to two Cys residues, such as is observed in the SCC variant, and eventually dissociates. This would explain both (1) the second phase observed in the CCC results compared to the SCC results and (2) the comparatively lower rates of $Hg(TNB)_2$ dissociation by the CAA and SAA variants. The conserved Cys93 residue near the corrinoid active site in HgcA is an interesting feature to speculate on in this regard as well, as it may serve some role in Hg(II) transfer to the active site rather than as a ligand to the cofactor.

The CAA and SAA variants are kinetically equivalent in this experiment, with slow rates of $Hg(TNB)_2$ dissociation, but comparatively high rates of TNB^- release in both observed phases. We interpret these data as indicative of adventitious Hg binding to the cluster Cys residues. Displacement of the cluster Fe atoms would be slower than binding to exposed C-terminal Cys residues, consistent with the slower observed rates of $Hg(TNB)_2$ decay. A chain reaction could be envisioned, depending on the solvent accessibility of the clusters, in which several Hg atoms adventitiously exchange one TNB- ligand for a nonspecific protein Cys and lead to an eventual collapse of the [4Fe-4S] cluster and sudden availability of Cys residues for binding and release of any TNB^- remaining associated with Hg(II). This model is speculative, but such a mechanism could be reconciled with the observed rapid rates for TNB^- release observed in the CAA and SAA variants, as well as the elevated rates of TNB^- release by the SAC and SCA variants.

Though the TNB^- and Cys thiolates in this experiment are sufficiently low in formal redox potential to reduce the Hg(II) ion, we do not believe that this contributes to the observed reactions under these conditions for two reasons: (1) the association constants for thiolate coordination of Hg(II) make complexation far more favorable than electron transfer[34], and (2) involvement of the TNB^- in thiol/disulfide redox chemistry would be reflected in the UV-visible spectrum of this experiment. For example, a scenario in which one equivalent of TNB^- is exchanged for one protein Cys residue, followed by reduction of Hg(II) and disulfide bond formation, would reflect only one equivalent of TNB^- released per $Hg(TNB)_2$, rather than the two equivalents observed in the Δ354nm and Δ408nm values. The low-potential [4Fe-4S] clusters seem more likely to be involved in Hg(II) reduction – this experiment, however, was conducted with as-purified oxidized clusters. No reductant is present in the system which could reduce the clusters for subsequent electron transfer to Hg(II), so this seems an unlikely explanation for the

kinetic traces observed. It has been proposed that a role for HgcB in electron transfer to Hg(II), rather than the HgcA corrinoid, could allow a carbocation mechanism to proceed in agreement with characterized cobalamin-dependent methylases, generating the observed $MeHg^+$. The Co(III)-C bond, however, is highly stable and only activated for carbocation transfer by nucleophilic attack of a substrate such as homocysteine[35] or the Ni-cluster of acetyl-CoA synthase[36] – Hg(0) is an inert metal and thus unlikely to induce the same chemistry.

2.4.4 Conclusions

This work has established a method for facile expression of HgcB as a MBP fusion protein in *E. coli*. UV-visible and EPR features of the purified protein are characteristic of [4Fe-4S] ferredoxins and the cluster UV-visible absorbance features can be titrated by addition of the low-potential chemical reductant, titanium (III) citrate. The requirement for titanium (III) citrate reduction over that of sodium dithionite indicates that the HgcB [4Fe-4S] clusters likely exhibit low midpoint redox potentials, which agrees with their putative role in 2 electron reduction of a corrinoid species. The consistency between the CCC (wild-type) protein reductive titration and the MHB Cys variants indicates that site-directed mutagenesis of these Cys residues does not adversely affect the incorporation or stability of the [4Fe-4S] clusters.

A bis-2-nitro-5-thiobenzoate Hg(II) complex ($Hg(TNB)_2$) was used as a colorimetric reporter of Hg(II) binding to MHB. Equilibrium titrations showed TNB^- release in great excess of the available protein thiols hypothesized to bind Hg(II); we interpreted this result as indicative of adventitious Hg(II) binding to the Cys residues involved in the [4Fe-4S] motifs, thus Hg(II) binding stoichiometry could not be obtained. The observation of this reaction by stopped-flow rapid kinetics indicated rapid dissociation of Hg(TNB)2 even in the absence of all three conserved Cys residues – this was unexpected and likely can also be attributed to nonspecific binding of Hg(II) to the cluster Cys residues. It can be concluded, however, that MHB variants containing two of the three conserved Cys residues, Cys73/Cys94/Cys95, induced the fastest rates of $Hg(TNB)_2$ dissociation, consistent with the Cys requirements for *in vivo* Hg methylation activity observed by *in vivo* mutagenesis experiments[13].

2.5 References for Chapter 2

(1) Parks, J. M.; Johs, A.; Podar, M.; Bridou, R.; Hurt Jr., R. A.; Smith, S. D.; Tomanicek, S. J.; Qian, Y.; Brown, S. D.; Brandt, C. C.; et al. The Genetic Basis for Bacterial Mercury Methylation. *Science.* **2013**, *339* (March), 1332–1336.

(2) Harris, R. C.; Rudd, J. W. M.; Amyot, M.; Babiarz, C. L.; Beaty, K. G.; Blanchfield, P. J.; Bodaly, R. A.; Branfireun, B. A.; Gilmour, C. C.; Graydon, J. A.; et al. Whole-Ecosystem Study Shows Rapid Fish-Mercury Response to Changes in Mercury Deposition. *Proc. Natl. Acad. Sci.* **2007**, *104* (42), 16586–16591.

(3) Clarkson, T. W. Critical Reviews in Toxicology The Toxicology of Mercury and Its Chemical Compounds. *Crit. Rev. Toxicol.* **2006**, *36* (8), 609–662.

(4) Matthews, R. G.; Koutmos, M.; Datta, S. Cobalamin-Dependent and Cobamide-Dependent Methyltransferases. *Curr. Opin. Struct. Biol.* **2008**, *18* (6), 658–666.

(5) Koay, M. S.; Antonkine, M. L.; Gärtner, W.; Lubitz, W. Modelling Low-Potential [Fe4S4] Clusters in Proteins. *Chem. Biodivers.* **2008**, *5* (8), 1571–1587.

(6) Banerjee, R. V.; Matthews, R. G.; Harder, S. R.; Ragsdale, S. W. Mechanism of Reductive Activation of Cobalamin-Dependent Methionine Synthase: An Electron Paramagnetic Resonance Spectroelectrochemical Study. *Biochemistry* **1990**, *29* (5), 1129–1135.

(7) Harder, S. R.; Lu, W. P.; Feinberg, B. A.; Ragsdale, S. W. Spectroelectrochemical Studies of the Corrinoid/Iron-Sulfur Protein Involved in Acetyl Coenzyme A Synthesis by Clostridium Thermoaceticum. *Biochemistry* **1989**, *28* (23), 9080–9087.

(8) Koutmos, M.; Datta, S.; Pattridge, K. a; Smith, J. L.; Matthews, R. G. Insights into the Reactivation of Cobalamin-Dependent Methionine Synthase. *Proc. Natl. Acad. Sci. U. S. A.* **2009**, *106* (44), 18527–18532.

(9) Nakamura, M.; Saeki, K.; Takahashi, Y. Hyperproduction of Recombinant Ferredoxins in Escherichia Coli by Coexpression of the ORF1-ORF2-IscS-IscU-IscA-HscB-HscA-Fdx-ORF3 Gene Cluster. *J Biochem* **1999**, *126*, 10–18.

(10) DeSilva, T. M.; Veglia, G.; Porcelli, F.; Prantner, A. M.; Opella, S. J. Selectivity in Heavy Metal-Binding to Peptides and Proteins. *Biopolymers* **2002**, *64* (4), 189–197.

(11) Barkay, T.; Miller, S. M.; Summers, A. O. Bacterial Mercury Resistance from Atoms to Ecosystems. *FEMS Microbiol. Rev.* **2003**, *27* (2–3), 355–384.

(12) Wang, D.; Huang, S.; Liu, P.; Liu, X.; He, Y.; Chen, W.; Hu, Q.; Wei, T.; Gan, J.; Ma, J.; et al. Structural Analysis of the Hg(II)-Regulatory Protein Tn501 MerR from Pseudomonas Aeruginosa. *Sci. Rep.* **2016**, *6* (August), 1–9.

(13) Smith, S. D.; Bridou, R.; Johs, A.; Parks, J. M.; Elias, D. A.; Hurt, R. A.; Brown, S. D.; Podar, M.; Wall, J. D. Site-Directed Mutagenesis of HgcA and HgcB Reveals Amino Acid Residues Important for Mercury Methylation. *Appl. Environ. Microbiol.* **2015**, *81* (9), 3205–3217.

(14) Zehnder, A. J. B.; Wuhrmann, K. Titanium (III) Citrate as a Nontoxic Oxidation-Reduction Buffering System for the Culture of Obligate Anaerobes Author (s): Alexander J . B . Zehnder and Karl Wuhrmann Source : Science , New Series , Vol . 194 , No . 4270 (Dec . 10 , 1976), Pp . 116. *Science (80-.).* **1976**, *194* (4270), 1165–1166.

(15) Cheng, Y.; Patel, D. J. An Efficient System for Small Protein Expression and Refolding. *Biochem. Biophys. Res. Commun.* **2004**, *317* (2), 401–405.

(16) Kapust, R. B.; Waugh, D. S. *Escherichia Coli* Maltose-Binding Protein Is Uncommonly Effective at Promoting the Solubility of Polypeptides to Which It Is Fused. *Protein Sci.* **1999**, *8* (8), 1668–1674.

(17) DelProposto, J.; Majmudar, C. Y.; Smith, J. L.; Brown, W. C. Mocr: A Novel Fusion Tag for Enhancing Solubility That Is Compatible with Structural Biology Applications. *Protein Expr. Purif.* **2009**, *63* (1), 40–49.

(18) Eschenfeldt, W. H.; Stols, L.; Millard, C. S.; Joachimiak, A.; Donnelly, I. A Family of LIC Vectors for High-Throughput Cloning and Purification of Proteins. **2009**, *498*, 105–115.

(19) Jeoung, J.-H.; Dobbek, H. Carbon Dioxide Activation at the Ni,Fe-Cluster of Anaerobic Carbon Monoxide Dehydrogenase. *Science.* **2007**, *317*, 490–494.

(20) Lanz, N. D.; Grove, T. L.; Gogonea, C. B.; Lee, K. H.; Krebs, C.; Booker, S. J. *RlmN and AtsB as Models for the Overproduction and Characterization of Radical SAM Proteins*, 1st ed.; Elsevier Inc., 2012; Vol. 516.

(21) Bradford, M. M. A Rapid and Sensitive Method for the Quantitation of Microgram Quantities of Protein Utilizing the Principle of Protein-Dye Binding. *Anal. Biochem.* **1976**, *72* (1–2), 248–254.

(22) Boll, M.; Fuchs, G. Identification and Characterization of the Natural Electron Donor Ferredoxin and of FAD as a Possible Prosthetic Group of Benzoyl-CoA Reductase (Dearomatizing), a Key Enzyme of Anaerobic Aromatic Metabolism. *Eur. J. Biochem.* **1998**, *251* (3), 946–954.

(23) Ledwidge, R.; Patel, B.; Dong, A.; Fiedler, D.; Falkowski, M.; Zelikova, J.; Summers, A. O.; Pai, E. F.; Miller, S. M. NmerA, the Metal Binding Domain of Mercuric Ion Reductase, Removes Hg 2+ from Proteins, Delivers It to the Catalytic Core, and Protects Cells under Glutathione-Depleted Conditions.

Biochemistry **2005**, *44* (34), 11402–11416.
(24) Carter, E. L.; Ramirez, Y.; Ragsdale, S. W. The Heme-Regulatory Motif of Nuclear Receptor Rev-Erbβ Is a Key Mediator of Heme and Redox Signaling in Circadian Rhythm Maintenance and Metabolism. *J. Biol. Chem.* **2017**, *292* (27), 11280–11299.
(25) Sweeney, W. V; Rabinowitz, J. C. PROTEINS CONTAINING 4Fe-4S CLUSTERS: AN OVERVIEW. *Annu. Rev. Biochem.* **1980**, *49*, 139–161.
(26) Seefeldt, L. C.; Ensign, S. A. A Continuous, Spectrophotometric Activity Assay for Nitrogenase Using the Reductant Titanium(III) Citrate. *Anal. Biochem.* **1994**, *221* (2), 379–386.
(27) Hagen, W. R. EPR SPECTROSCOPY OF IRON-SULFUR PROTEINS. In *Advance in Inorganic Chemistry*; 1992; Vol. 38, pp 165–222.
(28) Lovenberg, W.; Buchanon, B. B.; Rabinowitz, J. C. Studies on the Chemical Nature of Clostridial Ferredoxin. *J. Biol. Chem.* **1963**, *238* (12), 3899–3913.
(29) Lavoie, S. P.; Mapolelo, D. T.; Cowart, D. M.; Polacco, B. J.; Johnson, M. K.; Scott, R. A.; Miller, S. M.; Summers, A. O. Organic and Inorganic Mercurials Have Distinct Effects on Cellular Thiols, Metal Homeostasis, and Fe-Binding Proteins in Escherichia Coli. *J. Biol. Inorg. Chem.* **2015**, *20* (8), 1239–1251.
(30) Ellman, G. L. Tissue Sulfhydryl Groups. *Arch. Biochem. Biophys.* **1959**, *82*, 70–77.
(31) Ragsdale, S. W.; Lindahl, P. A.; Munck, E. Mossbauer, EPR, and Optical Studies of the Corrinoid/Iron-Sulfur Protein Involved in the Synthesis of Acetyl Coenzyme A by Clostridium Thermoaceticum. *J. Biol. Chem.* **1987**, *262* (29), 14289–14297.
(32) Cheesman, B. V.; Arnold, A. P.; Rabenstein, D. L. Nuclear Magnetic Resonance Studies of the Solution Chemistry of Metal Complexes. XV. Trimethyllead Complexes of Inorganic Ligands. *J. Am. Chem. Soc.* **1988**, *110*, 6359–6364.
(33) Miller, S. M.; Ballou, D. P.; Massey, V.; William, C. H. Two-Electron Reduced Mercuric Reductase Binds Hg(II) to the Active Site Dithiol but Does Not Catalyze Hg(II) Reduction. *J. Biol. Chem.* **1986**, *261* (18), 8081–8084.
(34) Stricks, W.; Kolthoff, I. M. Reactions between Mercuric Mercury and Cysteine and Glutathione. Apparent Dissociation Constants, Heats and Entropies of Formation of Various Forms of Mercuric Mercapto-Cysteine and -Glutathione. *J. Am. Chem. Soc.* **1953**, *75* (22), 5673–5681.
(35) Gruber, K.; Kratky, C.; Messerschmidt, A.; Huber, R.; Poulos, T.; Wieghardt, K.; Gruber, K.; Kratky, C. Cobalamin-Dependent Methionine Synthase. **2001**.
(36) Lu, W. P.; Harder, S. R.; Ragsdale, S. W. Controlled Potential Enzymology of Methyl Transfer Reactions Involved in Acetyl-CoA Synthesis by CO Dehydrogenase and the Corrinoid/Iron-Sulfur Protein from Clostridium Thermoaceticum. *J. Biol. Chem.* **1990**, *265* (6), 3124–3133.

Chapter 3 HgcA

3.1 Introduction

As discussed in Chapter 1 of this work, corrinoid-dependent proteins catalyze a variety of reactions, including methyl transfer[1]. Their functions and reactivity are tuned by the protein environment around the cofactor and protein ligand coordation (or lack of). Corrinoid-dependent methyltransferases typically bind corrinoid cofactors in a "base-off" mode, in which the dimethylbenzimidazole (DMB), or base, moiety coordinating the alpha axial face of the central Co atom dissociates and binds within a protein Rossmann fold[2]. Methionine synthase (MetH) provides a His ligand to the cofactor[3], but the corrinoid iron-sulfur protein (CFeSP) does not[4]. BtuM has been recently shown to coordinate one axial position with a Cys residue, the first example of such a coordination within a protein[5]. A light-dependent transcriptional regulator, CarH, binds in a "base-off, bis-His" motif, in which two His ligands coordinate both axial positions[6]. The crystal structures of these cobalamin binding modes are depicted in Figure 2.1 below.

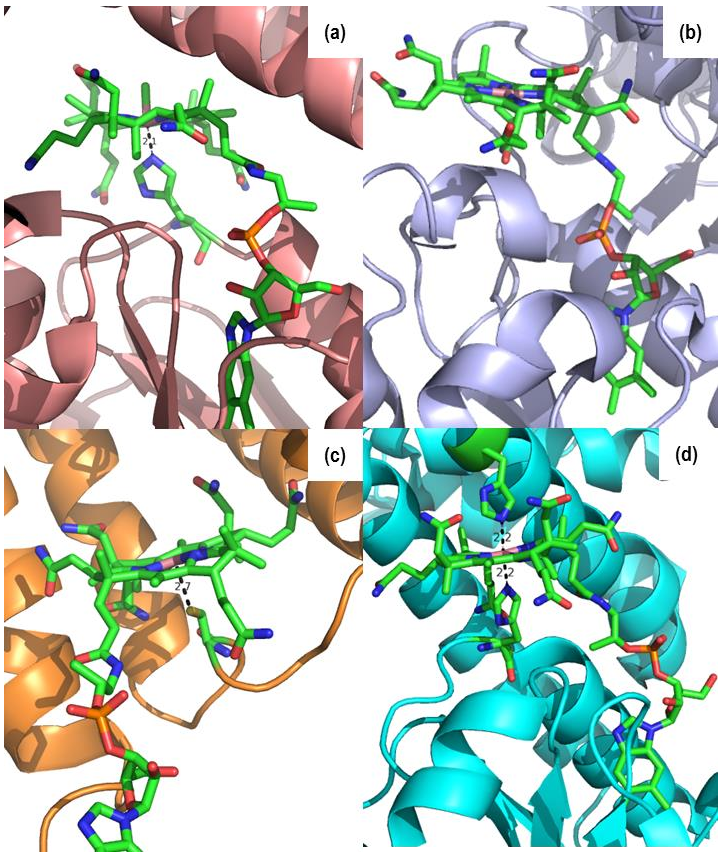

Figure 3.1 Crystal structures of observed "base-off" cobalamin protein binding modes (a) "base-off, His-on" methionine synthase (MetH) (b) "base-off" corrinoid iron-sulfur protein (CFeSP) (c) "base-off, Cys-on" vitamin B12 membrane transporter (BtuM) (d) "base-off, bis-His" light-dependent transcriptional regulator (CarH). The proteins are represented as cartoons while the cobalamin and relevant protein ligands are represented as sticks and colored by element. Rendered with Pymol from Protein Data Bank entries (a) 1BMT, (b) 4DJD, (c) 6FFV, and (d) 58CF.

HgcA is a 40kDa corrinoid protein with a C-terminal transmembrane (TM) domain which has been implicated as the mercury methylase in methylmercury biosynthesis[7]. Based on sequence similarity to the CFeSP, homology modelling suggests that a Cys residue at position 93 could coordinate to the "base-off" cofactor. We hypothesize this coordination would have a dramatic effect on the electronic environment and the mechanism of Co-C bond cleavage in the methylation reaction[8], potentially rationalizing the proposed transfer mechanism in which a methyl anion, in a departure from characterized Cbl-dependent methyltransferases, is transferred to Hg(II)[7]. Cys93 has been shown to be critical to Hg methylation in *Desulfovibrio desulfuricans* ND132 in an *in vivo* site-directed mutagenesis study[9]. This work identified several other requirements for native functional competency of the *hgcAB* system, including the HgcA TM

domain – deletion of this region of the *hgcA* gene eliminated *in vivo* Hg methylation, indicating that it is required for MeHg biosynthesis in some capacity. Our current functional understanding of HgcA, therefore, lacks direct functional assignment of key features which could be supplied by *in vitro* study.

HgcA is present at low levels in *Desulfovibrio desulfuricans* ND132[10] and *Geobacter sulfurreducens* PCA[11], thus it would be impractical to isolate quantities of protein required for *in vitro* characterization from these native sources. Heterologous expression of cobalamin-binding proteins, however, can present a significant technical challenge. Commonly used *Escherichia coli* derivative strains (BL21, C41, etc.) do not contain *de novo* corrinoid biosynthesis pathways, nor do they have a significant requirement for cobalamin under standard laboratory growth conditions[12]. Cobalamin uptake in *Escherichia coli* is tightly regulated by the binding of cobalamin to the mRNA encoding the cobalamin uptake gene, *btuB*, ensuring its transcription is not initiated when the cell's need for cobalamin is met[13]. This presents a barrier to heterologous expression of enzymes which require corrinoid cofactors for folding, stability, and/or solubility, as this regulation ensures there is not sufficient intracellular cobalamin available for binding.

In this work, two approaches were taken to heterologous production of cobalamin-replete HgcA. We first generated a panel of N- and C-terminally truncated variants of the HgcA soluble domain (lacking the predicted TM helices beginning approximately at position 175) and attempted cofactor reconstitution. Several variants were found to have enhanced solubility in comparison to HgcA-1-166, the construct purified as reported in Ref. 7, but none could be purified containing cobalamin or reconstituted with cofactor. The soluble truncated HgcA constructs exhibit UV-visible spectral shifts when added to Cbl, but cofactor reconstitution was assessed by electron paramagnetic resonance (EPR) spectroscopy to more definitively assess the Cbl coordination environment. "Base-on" cobalamin exhibits characteristic EPR spectral features arising from the interaction with the DMB nitrogen; the nuclear spin of the coordinating nitrogen atom causes superhyperfine splitting of EPR spectral features absent in the "base-off" configuration. EPR analysis of all constructs with which reconstitution was attempted indicated that the cofactor was still "base-on".

We reasoned that this inability to bind Cbl could arise from the removal of the TM domain. TM proteins present their own hurdles to heterologous overexpression, but advances in TM protein expression and extraction are constantly being made[14–16] and we sought to test the

hypothesis that the full-length (FL) protein is required to bind cofactor. In early 2018, a method for heterologous expression of cobalamin-binding proteins was published involving co-expression with a plasmid copy of the endogenous E. coli *btu* operon[17]. This operon is responsible for cobalamin uptake and encodes the outer membrane transporter BtuB, periplasmic chaperone BtuF, as well as BtuC and BtuD which are responsible for inner membrane trafficking into the cytosol. The TonB-dependent cobalamin transporter, *btuB*, has been show to contain a premature stop codon in BL21-derived laboratory research strains[18], rendering it dysfunctional, so the endogenous *btu* machinery cannot easily be exploited for the purposes of increases cellular Cbl uptake. By utilizing an inducible copy of the *btu* operon, we reasoned that an increase in the intracellular cobalamin pool could increase the likelihood of holo-FL-HgcA expression. Both FL-HgcA and HgcA-1-175 were co-expressed and purified from C41(DE3) cells in the presence of membrane-solubilizing detergents. The full-length and truncated proteins purified were characterized by SDS-PAGE analysis and UV-visible spectroscopy was used to compare the preliminary electronic features of the holo protein to known corrinoid proteins.

3.2 Materials and Methods

3.2.1 Materials

All chemicals were purchased from Sigma-Aldrich (St. Louis, MO) unless otherwise stated. All custom synthesized oligonucleotide primers were ordered from Integrated DNA Technologies (Coralville, Iowa). The FL-HgcA gene was custom synthesized into a pJ411 vector by DNA2.0 (Newark, CA). Pfu Ultra polymerase was purchased from Agilent (Santa Clara, CA). All restriction enzymes, T4 DNA ligase, and amylose affinity resin were procured from New England Biolabs (Ipswich, MA). TOP10 and BL21(DE3) chemically competent cells were purchased from Invitrogen/Life Technologies (Carlsbad, CA), and C41(DE3) chemically competent cells were purchased from Lucigen (Middleton, WI). cOmplete EDTA-free protease inhibitor tablets were acquired from Roche (Indianapolis, IN). The pET-Duet-1 vector was purchased from Novagen (Madison, WI) and the pBAD42-BtuCEDFB plasmid was a gift from the laboratory of Prof. Squire Booker, Pennsylvania State University. Ni-NTA resin and all DNA purification kits used between cloning steps (QIAquick gel extraction kit, QIAprep spin miniprep kit, QIAquick PCR purification kit) are from Qiagen (Valencia, CA).

3.2.2 HgcA 1-166: EPR spectroscopy

HgcA-1-166 samples for EPR spectroscopic analysis were prepared and supplied by Dr. Stephen Tomanicek and Dr. Alexander Johs (Oak Ridge National Laboratory). The protein was purified as described in Ref. 7, added to a stoichiometric amount of aquacobalamin, and exchanged into 25mM Na HEPES pH 7.5 at a concentration of 90uM. Reduction of Cbl was performed by the addition of 4 equivalents of sodium ascorbate to generate the Co(II) oxidation state. Two Cbl control samples were prepared by the same method: a "base-on" and a "base-off" sample, the latter of which contained 0.1M HCl.

Maltose binding protein (MBP) fusion constructs of HgcA-1-166 were also prepared and analyzed by EPR. In addition to the wild-type 1-166 sequence, a construct was generated in which two non-conserved Cys residues found in the HgcA sequence at positions 47 and 142 (SCS) were substituted with serine. These samples were prepared in the same buffer system as above, but Cbl reconstitution was carried out by addition of stoichiometric methylcobalamin (MeCbl). MeCbl was photolyzed by exposure to ambient light to generate the Co(II) oxidation state and a control MeCbl sample was prepared by the same method. These samples were found to be oxidized after shipping and reduced with two equivalents of titanium (III) citrate.

3.2.3 HgcA truncated constructs: design and ligation-independent cloning of HgcA variants

N-terminal truncations:	
GPVPRVRTYLRRDDRVGDLRARLGTNRHDFKVV**P**GLY…	(10-166)
PRVRTYLRRDDRVGDLRARLGTNRHDFKVV**P**GLY…	(13-166)
TYLRRDDRVGDLRARLGTNRHDFKVV**P**GLY…	(17-166)
GTNRHDFKVV**P**GLY…	(33-166)
FKVV**P**GLY…	(39-166)
PGLY…	(43-166)
C-terminal truncations:	
…P**A**FLRN	(33-162)
…P**A**FLRNGNKA	(33-166)
…P**A**FLRNGNKADEAMRGVTF	(33-175)

Figure 3.2 Start and end positions of HgcA truncated constructs. Bolded residues (Pro43 and Ala166) indicate the start and end positions of HgcA homology to CFeSP.

HgcA constructs were amplified from a commercially custom-synthesized pJ411 plasmid containing the FL-HgcA gene from *Desulfovibrio desulfuricans* ND132. This construct was codon-optimized for expression in *Escherichia coli*. Ligation-independent cloning (LIC) procedures were used to amplify HgcA variants with different combinations start and end positions and insert these constructs into the pMCSG7 vector and a modified pMCSG9 vectors[19]. These vectors contain N-terminal sequences encoding His_6 and His_6-MBP tags, respectively. Site-directed mutagenesis according to the Agilent QuikChange Site Directed Mutagenesis protocol was used to remove the His_6 tag from pMCSG9 prior to its assembly with the HgcA constructs, with the resulting vector designated pMCSG9-NH. Sequences were verified by Sanger sequencing using the T7 terminator primer (University of Michigan DNA Sequencing Core).

3.2.4 HgcA truncated constructs: expression/solubility tests and purification

His_6-HgcA constructs contained in the pMCSG7 vector were transformed into BL21(DE3) cells. 50mL cultures containing LB medium and 100ug/mL ampicillin were inoculated from glycerol stocks and grown at 37ºC with 225rpm shaking. HgcA expression was induced for 3 hours at 37ºC with 1mM IPTG at OD_{600} ~0.7. Gel samples were prepared from these cultures before and 3 hours after induction by resuspending a cell pellet prepared by centrifugation (5 min, 5,000xg) in 100uL 1X LDS loading buffer. These gel samples were analyzed by SDS-PAGE using 12.5% polyacrylamide gels. The cultures were harvested by centrifugation at 5,000xg for 15 minutes and stored at -20ºC. To test solubility after cell lysis, each frozen cell pellet was resuspended in 5mL lysis buffer (50mM Tris pH 7.8, 100mM NaCl, 5mM DTT, 1 Complete EDTA-free protease tablet per 50mL) and sonicated at 4ºC. A 100uL aliquot of each lysate was centrifuged in a benchtop microcentrifuge at 17,000xg for 10 minutes, and samples of the soluble and insoluble fractions were prepared for SDS-PAGE analysis.

MBP-HgcA constructs 39-166, 43-166, and 33-175 were expressed as above in 1L cultures, but induction was carried out overnight (18 hours) at 15ºC. These cell pellets were harvested and frozen at -20ºC prior to lysis and purification. Cell lysis and amylose affinity purification were conducted under anoxic conditions (< 1ppm oxygen) in a Vacuum Atmospheres anaerobic glove box. Pellets were thawed in 50mL lysis buffer containing 50mM Na HEPES pH 7.5, 100mM NaCl, 5mM DTT, and 1 protease inhibitor tablet. The resuspended

cells were lysed by sonication at 4ºC and the lysate cleared by centrifugation at 100,000xg. The soluble lysate was immediately applied to an amylose affinity column equilibrated with 5 column volumes (CV) of 25mM Na HEPES pH 7.5 and 5mM DTT. 2.5CV of this buffer was used to wash the column and MHB was eluted with the same buffer containing 20mM maltose. The purified protein was analyzed for homogenaity by SDS-PAGE.

3.2.5 HgcA truncated constructs: cobalamin reconstitution analysis by UV-visible spectroscopy

All sample handling and data collection was conducted inside an anaerobic glove box. Purified MBP-HgcA constructs were exchanged into 50mM Na HEPES pH 7.5 in centrifugal concentrators with a 30kDa molecular weight cut off (MWCO) membrane for cofactor addition. Aquacobalamin was added to purified MBP-HgcA constructs at a 0.9:1 ratio, to ensure spectral shifts observed did not arise from unbound cofactor. Protein concentrations for this purpose were determined by Bradford assay[20]. UV-visible spectra were collected using an Agilent/HP 8453 UV-visible spectrophotometer.

3.2.6 FL-HgcA: restriction digest cloning into pET-Duet-1

The FL-HgcA coding region and a truncated HgcA-1-175 construct were amplified by the polymerase chain reaction (PCR) from a custom synthesized, codon-optimized FL-HgcA vector (pFL-HgcA) with overhangs containing the BamHI and HindIII restriction enzyme sites. The PCR products and pET-Duet-1 vector were digested with both restriction enzymes, mixed and ligated using T4 DNA ligase, and transformed into TOP10 cells, generating the Duet-FL-HgcA and Duet-HgcA-1-175 vectors. Sequences were verified by Sanger sequencing (University of Michigan DNA Sequencing Core). Each HgcA plasmid was co-transformed into C41(DE3) cells with pBAD42-BtuCEDFB and plated on LB agar selection plates containing 100ug/mL ampicillin and 25ug/mL spectinomycin (50% working concentration).

3.2.7 FL-HgcA: co-expression with pBAD42-btuCEDFB and Ni-NTA affinity purification

Overnight starter cultures of C41(DE3) co-expression strains containing pBAD42-btuCEDFB and either Duet-FL-HgcA (pFL/pBtu) or Duet-HgcA-1-175 (p175/pBtu) were inoculated from single colonies in LB medium with 100ug/mL ampicillin and 50ug/mL spectinomycin. 100mL of the M9-ethanolamine media recipe described in Blaszczyk et.al.[20] was

prepared and inoculated with 0.75mL of the LB starter culture. HgcA expression was induced at OD_{600} ~0.7 overnight (16-18 hours) at 20ºC with 0.1 mM IPTG. Cells were harvested by centrifugation at 5,000xg and frozen at -20ºC. All purification steps were conducted in a cold room at 4ºC. Cell pellets were resuspended in 5mL lysis buffer containing 50mM KPi pH 7.4, 100mM sodium chloride, 10% glycerol, cOmplete EDTA-free protease inhibitor, 2mM β-mercaptoethanol (BME). The lysis buffer for the FL-HgcA strain also contained 1% N-lauryl sarcosine. Cells were lysed by sonication and centrifuged at 10,000xg for 30 minutes. 10mM imidazole was added to each soluble fractions and 2% Triton X-100 was added only to the FL-HgcA preparation. Each lysate was applied to Ni-NTA resin equilibrated in 50mM KPi pH 7.4, 100mM NaCl, 10% glycerol, 2mM BME and incubated with gentle shaking for 30 minutes. Each batch of resin was poured into a column and washed with 5CV of the equilibration buffer, and 250mM imidazole was included with 2CV of the same buffer to elute protein bound to the column. Protein eluted from each column was assessed by UV-visible spectroscopy to determine if it was purified with bound cofactor.

3.2.8 FL-HgcA: sample preparation for analysis by UV-visible spectroscopy

FL-HgcA for UV-visible and EPR analyses was purified as in section 3.2.7 with the following exceptions: 3L of cells expressing pFL/pBtu were grown and lysed in 75mL lysis buffer, and 4mM imidazole, rather than 10mM imidazole, was added to the soluble lysate. The column elution was concentrated in a centrifugal concentrator with a 10kDa MWCO. The concentrated FL-HgcA was exchanged three times with the same buffer used for Ni-NTA column equilibration in section 3.2.7. The flow through the centrifugal concentrator was pink in color and analyzed by UV-visible spectroscopy along with the concentrated protein. UV-visible spectra were collected with a Shimadzu UV-2600 spectrophometer.

3.3 Results and Analysis

3.3.1 HgcA-1-166 constructs: EPR spectra

The EPR spectrum of HgcA-1-166 in Figure 3.3a closely resembles that of "base-on" Cbl (Figure 3.3b), with g values ~2.0 and ~2.3. Hyperfine splitting constants for cobalt and nitrogen in both of these species were calculated as A_{Co} = 110G and A_N = 18G. The acidified "base-off" Cbl sample (Figure 3.3c), in which protonation and dissociation of the DMB lower axial ligand

is promoted, exhibits no nitrogen superhyperfine splitting lines and a broadened A_{Co} = 155G, typical of "base-off" corrinoid species[4,22]. Thus it was concluded that cobalamin addition to HgcA-1-166 does not yield a "base-off" reconstituted protein. EPR spectra of the MBP-HgcA variants in Figure 3.3d-e exhibit virtually identical features to the "base-on" spectra in Figure 3.3a and f.

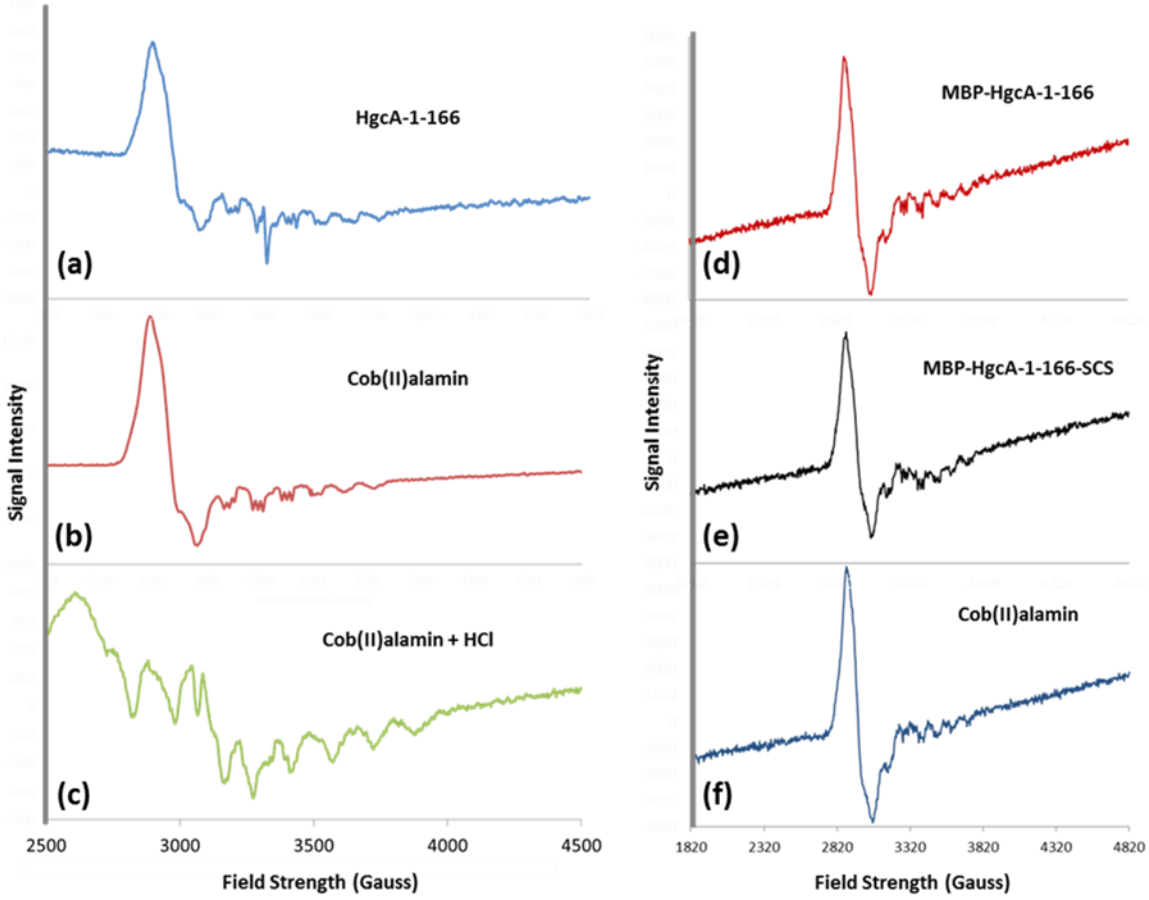

Figure 3.3 EPR spectra of HgcA-1-166 constructs compared to "base-on" and "base-off" cobalamin. All EPR data collection parameters: 20mW power, 10G amplitude modulation, $7x10^4$ gain, and 9.28 GHz frequency at 100K. (a) HgcA-1-166 (b) cob(II)alamin (c) cob(II)alamin in 0.1M HCl. Samples a-c were prepared as described in Section 3.2.2 by reduction with sodium ascorbate. (d) MBP-HgcA-1-166 (e) MBP-HgcA-1-166 SCS, in which two nonconserved Cys residues are mutated to serine (f) cob(II)alamin. A cob(II)alamin spectrum appears in each set of samples as a control comparison (a and f).

3.3.2 HgcA truncated constructs: SDS-PAGE analysis of construct expression and solubility

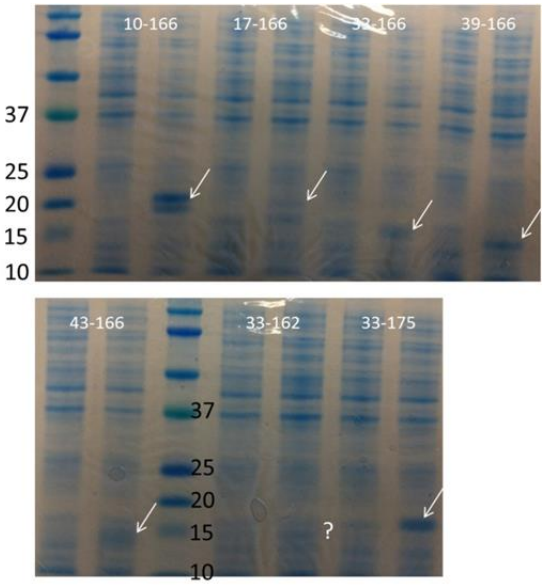

Figure 3.4 HgcA truncated construct expression test analysis by SDS-PAGE. Lanes with numbered bands contain molecular weight standards. Constructs are labelled as pairs of gel lanes where the left lane corresponds to a pre-induction gel sample and the right lane corresponds to a post-induction gel sample of equivalent cell density.

The molecular weights of the HgcA truncated constructs range from 13.8kDa – 17.7kDa. The SDS-PAGE analysis in Figure 3.4 indicates the presence of band of appropriate molecular weight band in each of the 7 test expressions, marked by a white arrow, with the exception of 33-162, which was inconclusive. These constructs include N-terminal His tags but no fusion tag to promote solubility, so their solubility after lysis was assessed in Figure 3.5. The same cells were lysed and their corresponding soluble and insoluble fractions were analyzed by SDS-PAGE in Figure 3.5.

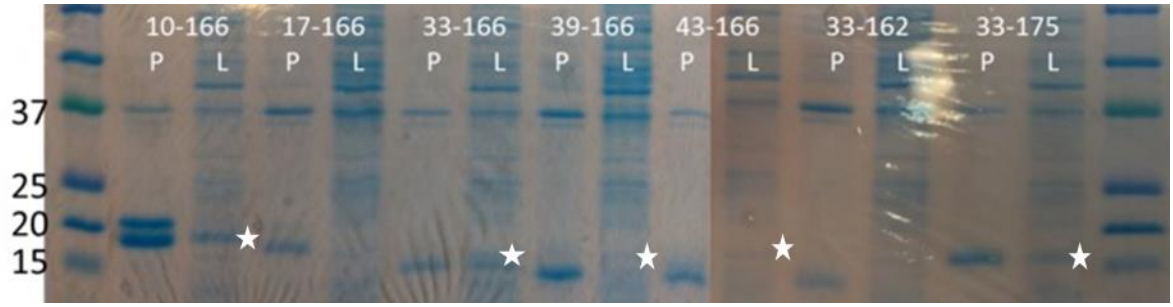

Figure 3.5 SDS-PAGE analysis of HgcA truncated construct solubility after cell lysis. "P" and "L" lanes designated for each construct correspond to the insoluble pellet and soluble cell

extract, respectively. White stars to the right of a gel band indicate a band of the appropriate molecular weight in the soluble lysate fraction.

HgcA-39-166, HgcA-43-166, and HgcA-33-175 were chosen for expression purification as MBP fusion constructs on the basis of the results in Figure 3.5. Figure 3.6 shows samples taken throughout the lysis and amylose affinity purification of MBP-HgcA-43-166 and is representative of all purifications of these constructs. The protein eluted from the amylose affinity column can be seen in the rightmost gel lanes (Fractions 1-3). The amylose affinity eluate contains minor contaminating bands, but appears mostly pure and was used for subsequent cofactor addition experiments.

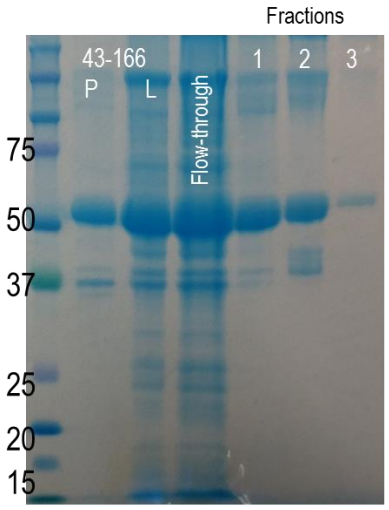

Figure 3.6 MBP-HgcA-43-166 amylose affinity purification analysis by SDS-PAGE. The numbered lane contains molecular weight standards. P and L represent the soluble and insoluble fractions of the cell lysate. The lane labelled "flow-through" contains the column flow collected as the soluble lysate was loaded on an amylose affinity column, and fractions 1-3 are the amylose column eluate.

3.3.3 HgcA truncated constructs: UV-visible spectral analysis of cobalamin reconstitution

Substoichiometric (0.9:1) addition of to the purified MBP-HgcA variants yielded changes to the UV-visible spectrum. The 43-166 and 33-175 variants exhibit a feature at 475nm, which typically identifies "base-on" cob(II)alamin[23]. The 500nm region is red-shifted in the 39-166 construct with a peak at 530nm; this feature is generally seen in glutathionylcobalamin, in which a thiolate ligand coordinates the β-axial position of "base-on" Cbl[24]. A spectrum of cob(III)alamin is provided as a reference for the species added to the proteins. These data are consistent with either (a) reduction of the cobalamin, likely by reduced surface Cys residues of

HgcA, in the cases of 43-166 and 33-175 or (b) the association of "base-on" Cbl with a protein Cys residue via β-axial coordination. There is no indication in these spectral changes of a "base-off" reconstituted HgcA.

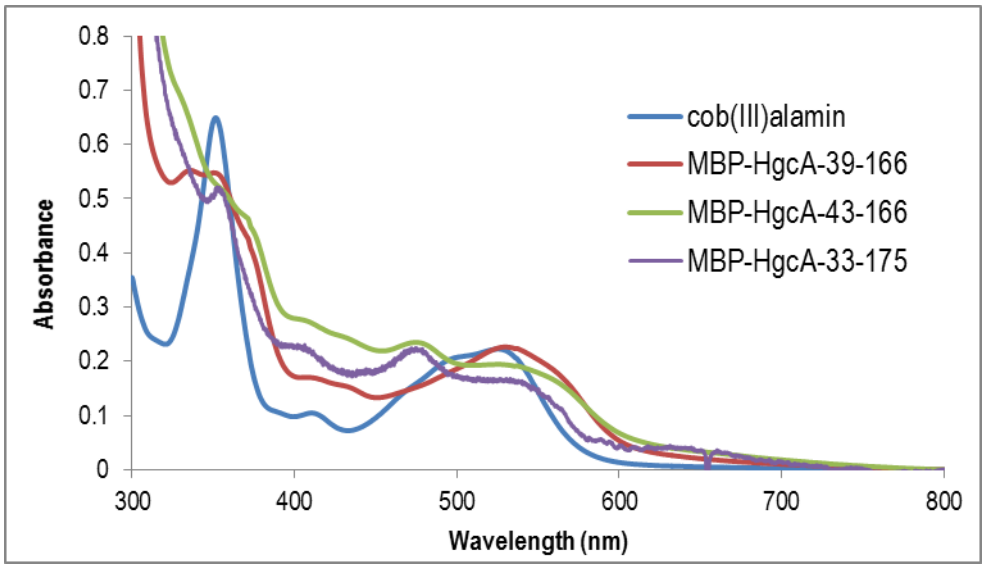

Figure 3.7 UV-visible spectra of HgcA MBP fusion constructs upon stoichiometric addition of aquacobalamin

3.3.4 FL-HgcA: Analysis of pBAD42-BtuCEDFB co-expression and affinity purification vs. HgcA-1-175

SDS-PAGE analysis of the Duet-FL-HgcA and Duet-HgcA-1-175 purification steps did not identify distinct bands of corresponding molecular weights (~40kDa and ~20kDa, respectively) to definitively assign to the two HgcA constructs (data not shown). The same analysis of the larger scale Duet-FL-HgcA expression (Figure 3.8) appears to indicate enrichment of an approximately 40kDa species, consistent with the molecular weight of FL-HgcA.

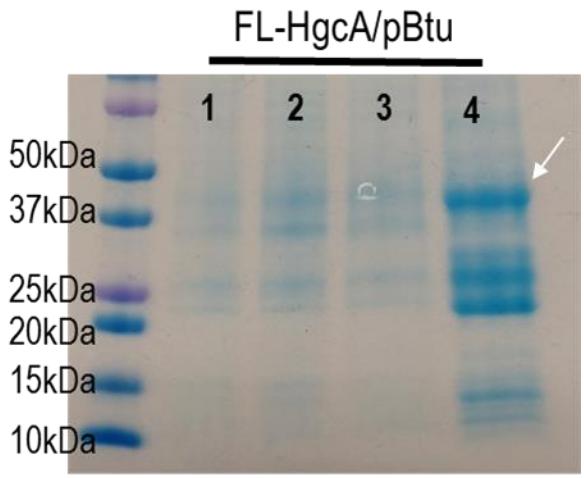

Figure 3.8 SDS-PAGE analysis of FL-HgcA co-expressed with pBAD-BtuCEDFB. (1) soluble cell extract after lysis and centrifugation (2) Ni-NTA column flow-through during application of lysate (3) Ni-NTA column wash (4) Ni-NTA column elution. The ~40kDa band in Lane 4 is thought to correspond to FL-HgcA and is marked with a white arrow. pBAD42-BtuCEDFB is abbreviated 'pBtu' for brevity.

The UV-visible spectra of FL-HgcA and HgcA-1-175 co-expressed with the pBAD42-BtuCEDFB plasmid and purified aerobically by Ni-NTA affinity chromatography are presented below in Figure 3.9. The UV-visible spectrum of HgcA-1-175 exhibits a peak at 358nm with shoulders around 402nm and 535nm. This spectrum is not distinctive, but could be consistent with aquacobalamin, which has a dominant transition at 360nm and a feature composed of two overlapping peaks at 515nm and 545nm[25]. A spectrum with peaks at 358nm, 414nm, and a broader feature which appears to contain peaks at ~538nm and ~562nm is seen in the peach-colored FL-HgcA elution. This is an unusual cobalamin spectrum – cob(III)alamin compounds generally exhibit a feature in the mid-300nm range and a broader set of transitions in the 500-550nm range, with molar extinction coefficients 2.5-3 times higher in the higher energy peaks[26]. The ~1:1 ratio between the 358nm peak and 412nm peak is not typical, as there are generally no major electronic transitions in the 400nm region at all, and cannot be assigned to a well-characterized cobalamin coordination environment.

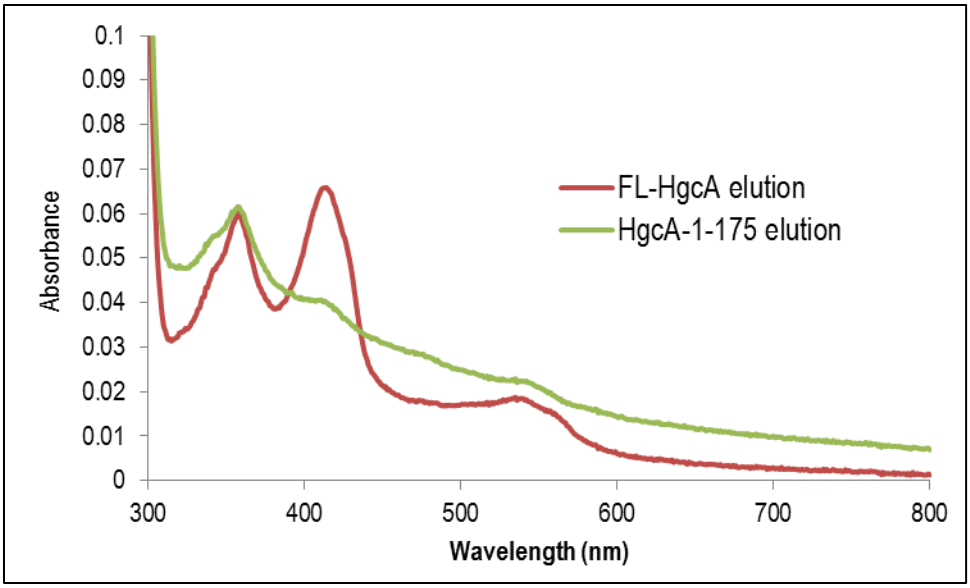

Figure 3.9 UV-visible spectra of Ni-NTA purified HgcA variants co-expressed with pBAD-BtuCEDFB. The FL-HgcA spectrum indicates maxima at 358nm and 414nm and a broad feature ~538nm and ~562nm. The HgcA-1-175 spectrum is not very distinct and displays a major peak at 358nm.

3.3.5 FL-HgcA: UV-visible spectrum

The FL-HgcA Ni-NTA column elution was concentrated in a centrifugal ultrafiltration device with a 10kDa MWCO membrane. The flow through the concentrator membrane was pink in color and its UV-visible spectrum is presented in Figure 3.10. This spectrum has well defined features with a maximum at 358nm which is ~3-fold higher in intensity than a shoulder around 540nm. This closely resembles published spectra of aquacobalamin[25,26], and likely represents cofactor nonspecifically associated with the purified FL-HgcA. The FL-HgcA spectrum, on the other hand, is characterized by a single broad feature with a maximum at 410nm and shoulder ~427nm, with some indication of the lower intensity Co(III) 500-550nm transitions. Reduction of both Cbl and cobinamide (Cbi), which lacks the lower axial DMB moiety, from Co(III) to Co(II) is accompanied by a loss of absorbance in the 500-550nm region and emergence of a feature at 475nm[23]. Though 412nm is significantly blue-shifted from this characterized state, this sample was frozen for EPR spectroscopic analysis to determine if it was in the Co(II) oxidation state. No EPR signal was detected, possibly due to insufficient concentration or an EPR-silent oxidation state (Co(III)). Though the FL-HgcA sample could not be definitively characterized, this simple experiment deconvoluted the spectrum observed in Figure 3.9 into two distinct species: aquacobalamin and some corrinoid coordination environment associated with FL-HgcA.

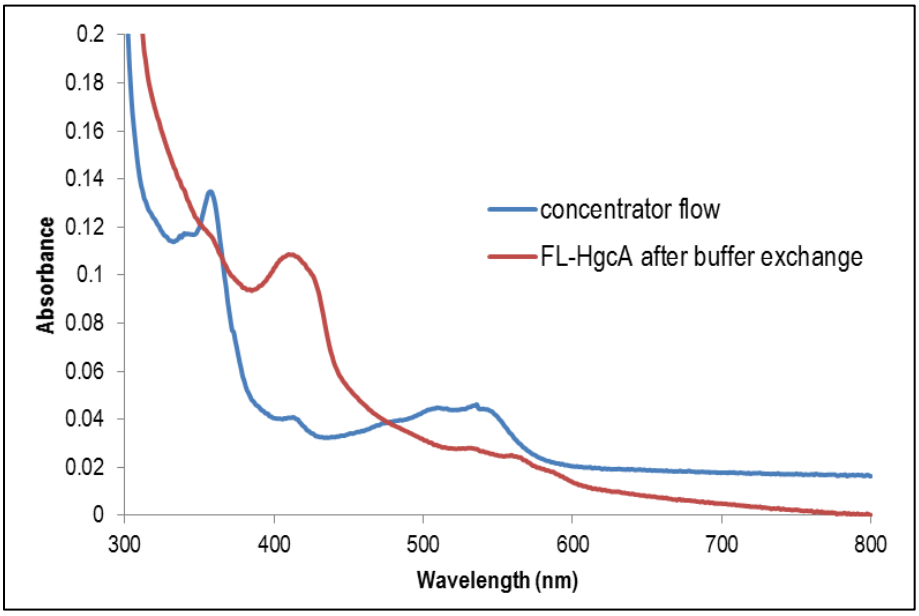

Figure 3.10 Deconvolution of Cbl species contributing to purified FL-HgcA spectrum. The centrifugal concentrator flow-through spectrum exhibits a maximum at 358nm and feature containing peaks ~515nm and 540nm. The FL-HgcA spectrum is characterized by a broad peak with a maximum at 410nm.

3.4 Discussion

3.4.1 HgcA-1-166 constructs do not bind "base-off" cobalamin

Parks et.al. reported the purification and cobalamin reconstitution of HgcA-1-166 and a variant in which Cys73, the residue predicted by homology modelling to coordinate the alpha axial position of the corrinoid cofactor, is mutated to a threonine (C93T)[7]. The UV-visible analysis of these constructs following stoichiometric addition of aqua-Cbl indicated shifts in the UV-visible spectrum, but the nature of these transitions was unclear. Dr. Stephen Tomanicek and Dr. Alexander Johs provided us with samples prepared in a similar manner for EPR analysis to better understand the Cbl coordination environment in these samples. The EPR spectra obtained in section 3.3.1 overlay with that of cob(II)alamin and the nitrogen superhyperfine triplet splitting observed indicates the "base-on" configuration. This suggests that Cbl associated with these samples is not coordinated to the HgcA-1-166 in a "base-off, Cys-on" mode. This clarifies the shifts observed in the UV-visible spectra as indicative of cobalamin association with the purified HgcA constructs or reduction by exposed Cys residues, but not cofactor incorporation

into HgcA in the hypothesized "base-off" mode. Furthermore, the MBP-HgcA-1-166 construct, which was more highly expressed and readily soluble, also was not reconstituted by addition of Cbl to purified protein.

3.4.2 Screen of HgcA truncated constructs

Truncation of proteins at the N- and C-termini[27] and/or removal of regions with predicted disorder[28] are common structural biology approaches to generate protein constructs suitable for large-scale expression and purification. The design of such constructs ranges from semi-rational to random screening, as the effect of seemingly minor alterations can dramatically impact protein solubility and stability. Here we identify that HgcA constructs lacking the C-terminal transmembrane domain are more readily soluble after truncation of 30+ residues of the N-terminus (Figure 3.6). The region of HgcA which exhibits high sequence similarity to the CFeSP is composed of residues 43-166 – the N-terminal 42 residues are highly positively charged and no function for this region has been proposed. However, these constructs are not reconstituted by *in vitro* addition of Cbl, in a similar result to the HgcA-1-166 construct. It has been observed by *in vivo* mutagenesis studies that genomic deletion of the HgcA transmembrane domain eliminates the host organism's capacity to synthesize MeHg[9]. Taken together, the *in vivo* data are consistent with the observations in this work that the N-terminal cytosolic domain is not competent to bind Cbl. However, the mechanism of Cbl incorporation into HgcA *in vivo* is not known – many examples of corrinoid proteins exist within the scientific literature which cannot be purified as soluble proteins from heterologous systems and reconstituted by simple addition of Cbl[17,29]. It may be that HgcA must encounter Cbl co-translationally or in the presence of a chaperone to incorporate "base-off" Cbl, regardless of the presence of the C-terminal transmembrane domain.

3.4.3 FL-HgcA and HgcA-1-175 exhibit different cobalamin spectra after co-expression with pBAD-BtuCDEFB

The acquisition of the pBAD42-BtuCEDFB co-expression system made it possible to test the hypothesis that the HgcA TM domain is required to bind Cbl. FL-HgcA and HgcA-1-175 were purified in the presence of the resulting exaggerated levels of intracellular cobalamin (See Figure 3.11). Both constructs were purified under the same conditions by Ni-NTA affinity chromatography and analyzed by UV-visible spectroscopy. The HgcA-1-175 truncated construct

displayed low intensity spectral features suggestive of aquaCbl in its UV-visible spectrum, whereas the purified FL-HgcA indicated a higher concentration of Cbl co-purified with the protein. In light of (a) these results, (b) the suggestion from HgcA *in vitro* reconstitution discussed in sections 3.4.1 and 3.4.2, and (c) the *in vivo* defect in MeHg biosynthesis after deletion of the HgcA TM domain observed by Smith et.al.[9], we conclude that neither addition of cobalamin to purified HgcA nor an increase in intracellular Cbl during expression result in purification of holo-HgcA because the HgcA transmembrane domain is structurally or conformationally required for cofactor binding.

3.4.4 UV-visible spectral features of FL-HgcA

After larger-scale purification of FL-HgcA and buffer exchange, the FL-HgcA spectrum in Figure 3.9 was deconvoluted into two components. One, with wavelength maxima at 358nm and 515nm/540nm, corresponds to an an oxidized cob(III)alamin, in which a high intensity peak near ~350nm and a lower intensity feature in the 500nm-550nm range are observed[26]. The other exhibits a single broad feature ~410nm and is not readily assigned to published spectra – the presence of the reductant BME in purification buffers may be sufficient to reduce the cobalamin to Co(II), but Co(II) corrinoid spectra are typically characterized by a feature at 475nm[23]. We are currently working to optimize the purification and detergent extraction of FL-HgcA to yield greater amounts of protein toward assigning this coordination environment.

3.4.5 Conclusions

Here we present a variety of attempts to heterologously express and purify HgcA. EPR analysis of HgcA-1-166 indicated that reported spectral shifts upon cofactor addition were not indicative of "base-off" incorporation into the protein. A panel of HgcA truncations was designed and constructs which exhibited robust heterologous expression and solubility after cell lysis were identified. These constructs were similarly unable to be reconstituted with Cbl *in vitro*. Heterologous expression of HgcA-1-175 was compared side-by-side with the full length HgcA protein in the presence of high intracellular Cbl, promoted by co-expression with an inducible copy of the *btu* genes. The truncated variant failed to co-purify with Cbl to the same level as the FL-HgcA, leading us to the conclusion that the C-terminal TM domain may be structurally or functionally required for Cbl binding to HgcA. The FL-HgcA exhibits an unusual UV-visible

spectrum which we hope will lend itself to further characterization and yield insight into the Cbl binding mode of HgcA.

3.5 References for Chapter 3

(1) Bridwell-Rabb, J.; Drennan, C. L. Vitamin B12 in the Spotlight Again. *Curr. Opin. Chem. Biol.* **2017**, *37*, 63–70.

(2) Matthews, R. G.; Koutmos, M.; Datta, S. Cobalamin-Dependent and Cobamide-Dependent Methyltransferases. *Curr. Opin. Struct. Biol.* **2008**, *18* (6), 658–666.

(3) Drennan, C. L.; Huang, S.; Drummond, J. T.; Matthews, R. G.; Ludwig, M. L. How a Protein Binds B_{12}: A 3.0 Å X-Ray Structure of B_{12}-Binding Domains of Methionine Synthase. *Science* **1994**, *266* (5191), 1669–1674.

(4) Ragsdale, S. W.; Lindahl, P. A.; Munck, E. Mossbauer, EPR, and Optical Studies of the Corrinoid/Iron-Sulfur Protein Involved in the Synthesis of Acetyl Coenzyme A by Clostridium Thermoaceticum. *J. Biol. Chem.* **1987**, *262* (29), 14289–14297.

(5) Rempel, S., Colucci, E., de Gier, J.W., Guskov, A., Slotboom, D. J. Cysteine-Mediated Decyanation of Vitamin B12 by the Predicted Membrane Transporter BtuM. *Nat. Commun.* **2018**, No. 2018, 1–8.

(6) Jost, M.; Fernandez-Zapata, J.; Polanco, M. C.; Ortiz-Guerrero, J. M.; Chen, P. Y. T.; Kang, G.; Padmanabhan, S.; Elias-Arnanz, M.; Drennan, C. L. Structural Basis for Gene Regulation by a B12-Dependent Photoreceptor. *Nature* **2015**, *526* (7574), 536–541.

(7) Parks, J. M.; Johs, A.; Podar, M.; Bridou, R.; Hurt Jr., R. A.; Smith, S. D.; Tomanicek, S. J.; Qian, Y.; Brown, S. D.; Brandt, C. C.; et al. The Genetic Basis for Bacterial Mercury Methylation. *Science.* **2013**, *339*, 1332–1336.

(8) Zhou, J.; Riccardi, D.; Beste, A.; Smith, J. C.; Parks, J. M. Mercury Methylation by HgcA: Theory Supports Carbanion Transfer to Hg(II). *Inorg. Chem.* **2014**, *53* (2), 772–777.

(9) Smith, S. D.; Bridou, R.; Johs, A.; Parks, J. M.; Elias, D. A.; Hurt, R. A.; Brown, S. D.; Podar, M.; Wall, J. D. Site-Directed Mutagenesis of HgcA and HgcB Reveals Amino Acid Residues Important for Mercury Methylation. *Appl. Environ. Microbiol.* **2015**, *81* (9), 3205–3217.

(10) Qian, C.; Chen, H.; Johs, A.; Lu, X.; An, J.; Pierce, E. M.; Parks, J. M.; Elias, D. A.; Hettich, R. L.; Gu, B. Quantitative Proteomic Analysis of Biological Processes and Responses of the Bacterium *Desulfovibrio Desulfuricans* ND132 upon Deletion of Its Mercury Methylation Genes. *Proteomics* **2018**, 1700479.

(11) Qian, C.; Johs, A.; Chen, H.; Mann, B. F.; Lu, X.; Abraham, P. E.; Hettich, R. L.; Gu, B. Global Proteome Response to Deletion of Genes Related to Mercury Methylation and Dissimilatory Metal Reduction Reveals Changes in Respiratory Metabolism in Geobacter Sulfurreducens PCA. *J. Proteome Res.* **2016**, *15* (10), 3540–3549.

(12) Lawrence, J. G.; Roth, J. R. Evolution of Coenzyme B12 Synthesis among Enteric Bacteria: Evidence for Loss and Reacquisition of a Multigene Complex. *Genetics* **1996**, *142* (1), 11–24.

(13) Nou, X.; Kadner, R. J. Adenosylcobalamin Inhibits Ribosome Binding to BtuB RNA. *Proc. Natl. Acad. Sci.* **2000**, *97* (13), 7190–7195.

(14) Wagner, S.; Bader, M. L.; Drew, D.; de Gier, J. W. Rationalizing Membrane Protein Overexpression. *Trends Biotechnol.* **2006**, *24* (8), 364–371.

(15) Grisshammer, R. Understanding Recombinant Expression of Membrane Proteins. *Curr. Opin. Biotechnol.* **2006**, *17* (4), 337–340.

(16) Denisov, I. G.; Sligar, S. G. Nanodiscs in Membrane Biochemistry and Biophysics. *Chem. Rev.* **2017**, *117* (6), 4669–4713.

(17) Lanz, N. D.; Blaszczyk, A. J.; McCarthy, E. L.; Wang, B.; Wang, R. X.; Jones, B. S.; Booker, S. J. Enhanced Solubilization of Class B Radical S-Adenosylmethionine Methylases by Improved Cobalamin Uptake in Escherichia Coli. *Biochemistry* **2018**, *57* (9), 1475–1490.

(18) Studier, F. W.; Daegelen, P.; Lenski, R. E.; Maslov, S.; Kim, J. F. Understanding the Differences between Genome Sequences of Escherichia Coli B Strains REL606 and BL21(DE3) and Comparison of the E. Coli B and K-12 Genomes. *J. Mol. Biol.* **2009**, *394* (4), 653–680.

(19) Eschenfeldt, W. H.; Stols, L.; Millard, C. S.; Joachimiak, A.; Donnelly, I. A Family of LIC Vectors for High-Throughput Cloning and Purification of Proteins. **2009**, *498*, 105–115.

(20) Bradford, M. M. A Rapid and Sensitive Method for the Quantitation of Microgram Quantities of Protein

Utilizing the Principle of Protein-Dye Binding. *Anal. Biochem.* **1976**, *72* (1–2), 248–254.
(21) Blaszczyk, A. J.; Wang, R. X.; Booker, S. J. *TsrM as a Model for Purifying and Characterizing Cobalamin-Dependent Radical S-Adenosylmethionine Methylases*, 1st ed.; Elsevier Inc., 2017; Vol. 595.
(22) Bayston, J.; Looney, F.; Pilbrow, J.; Winfield, M. Electron Paramagnetic Resonance Studies of Cob(II)Alamin and Cob(II)Inamides. *Biochemistry* **1967**, *9* (10), 32–41.
(23) Stich, T. A.; Buan, N. R.; Brunold, T. C. Spectroscopic and Computational Studies of Co2+corrinoids: Spectral and Electronic Properties of the Biologically Relevant Base-on and Base-off Forms of Co2+cobalamin. *J. Am. Chem. Soc.* **2004**, *126* (31), 9735–9749.
(24) Conrad, K. S.; Brunold, T. C. Spectroscopic and Computational Studies of Glutathionylcobalamin: Nature of Co-S Bonding and Comparison to Co-C Bonding in Coenzyme B 12. *Inorg. Chem.* **2011**, *50* (18), 8755–8766.
(25) Hill, J. A.; Pratt, J. M.; Williams, R. J. P. The Chemistry of Vitamin B12. Part I. The Valency and Spectrum of the Coenzyme. *J. Chem. Soc.* **1964**, 5149–5153.
(26) Stich, T. A.; Brooks, A. J.; Buan, N. R.; Brunold, T. C. Spectroscopic and Computational Studies of Co 3+ -Corrinoids: Spectral and Electronic Properties of the B 12 Cofactors and Biologically Relevant Precursors. *J. Am. Chem. Soc.* **2003**, *125* (19), 5897–5914.
(27) Gräslund, S.; Nordlund, P.; Weigelt, J.; Hallberg, B. M.; Bray, J.; Gileadi, O.; Knapp, S.; Oppermann, U.; Arrowsmith, C.; Hui, R.; et al. Protein Production and Purification. *Nat. Methods* **2008**, *5* (2), 135–146.
(28) Linding, R.; Jensen, L. J.; Diella, F.; Bork, P.; Gibson, T. J.; Russell, R. B. Protein Disorder Prediction: Implications for Structural Proteomics. *Structure* **2003**, *11* (11), 1453–1459.
(29) Lu, W. P.; Schiau, I.; Cunningham, J. R.; Ragsdale, S. W. Sequence and Expression of the Gene Encoding the Corrinoid/Iron-Sulfur Protein from Clostridium Thermoaceticum and Reconstitution of the Recombinant Protein to Full Activity. *J. Biol. Chem.* **1993**, *268* (8), 5605–5614.

Chapter 4 Conclusions and Future Directions

4.1 Conclusions

Both HgcA and HgcB contain metal cofactors which present challenges to heterologous production. As these proteins are expressed at low levels in two well-characterized model Hg methylating organisms, *Desulfovibrio desulfuricans* ND132[1]and *Geobacter sufurreducens* PCA[2], large-scale purification from these hosts appears a difficult and unattractive method. Here we present protocols for co-expression of these genes in *Escherichia coli* K12 derived strains with plasmid-encoded cofactor uptake and/or incorporation systems, developed by the Takahashi[3] and Booker[4] laboratories, respectively. While the maltose binding protein (MBP) affinity tag solubilizes the expressed HgcB and allows for facile affinity purification, our inability to remove the MBP tag from HgcB after proteolysis is a limitation of this method – this could be investigated by purification optimization or a different affinity tag could be used. Further optimization of HgcA purification could include its assembly into nanodiscs to better mimic its native transmembrane conformation[5]. Perhaps co-expression of HgcA and HgcB yields a stable protein complex and would stabilize/solubilize HgcB in the absence of the MBP tag; these efforts are ongoing in our laboratory. Nonetheless, these are the first successful protocols for expression and purification of HgcA and HgcB to our knowledge, and the ability to produce large quantities of these proteins will be critical to future *in vitro* characterization.

In Chapter 2, we show that heterologously expressed MBP-HgcB (abbreviated MHB) exhibits UV-visible characteristics typical of [4Fe-4S] cluster ferredoxins. Its UV-visible spectrum is redox-dependent and can be quenched by chemical reduction. The EPR spectrum of MHB revealed the feature centered at g = 1.94 indicative of [4Fe-4S] clusters. It is noteworthy that titanium (III) citrate was required to reduce MHB to the EPR-active +1 state, whereas dithionite reduced MHB did not exhibit an EPR spectrum, suggesting that the MHB [4Fe-4S] cluster potentials are quite low; this deserves further study as it could inform the *in vivo* ability of HgcB to transfer electrons to a low-potential (~500mV) corrinoid. Furthermore, UV-visible and EPR spectroscopic studies of a panel of Cys mutants of HgcB exhibit identical characteristics to

the wild-type construct, suggesting that their overall conformation is not adversely affected by Ser substitution of Cys73 and/or Ala substitution of Cys94 and Cys95.

A $Hg(TNB)_2$ titration[6] was used to probe the Hg(II) binding characteristics of MHB. Stopped-flow rapid kinetic experiments of the $Hg(TNB)_2$ interaction with MHB and a panel of variants in which combinations of the conserved Cys 73, Cys94, and/or Cys95 residues were substituted with Ala or Ser by site-directed mutagenesis. The data obtained indicated differential rates of $Hg(TNB)_2$ decay and TNB^- appearance between various sets of mutants. Briefly, the SCC variant was found to fit to the simplest model of Hg(II) binding in a single phase – this was taken as an indication that the Cys94/Cys95 pair bind stoichiometric Hg in the first step of the MHB:Hg interaction. Curiously, this was not consistent with the wild-type CCC variant, which exhibited a phase with a similar rate of $Hg(TNB)_2$ decay to the SCC ($\sim 100 s^{-1}$), but an additional phase was also observed in the fit to a double exponential model. This rate, also observed in the CAC and CCA mutants, we attribute to bidentate coordination of Hg(II) by HgcB, which appears to require two of the three relevant Cys residues. The slightly slower, though still rapid, decay of Hg(TNB)2 induced by CAA and SAA, which contain only Cys73 and no Cys residues, respectively, we attribute to nonspecific displacement of the iron-sulfur clusters by Hg(II) binding to the Cys residues involved in their coordination. These data provide insight into the hypothesis that these Cys residues comprise a Hg(II) binding site and deliver the Hg(II) substrate to the HgcA corrinoid for methylation, and are consistent with the observed *in vivo* requirement for Cys 73 and either Cys94 or Cys95 for Hg methylating activity[7].

FL-HgcA was purified in Chapter 3. As a series of HgcA constructs lacking the C-terminal transmembrane region could not be reconstituted *in vitro* with Cbl cofactor, a co-expression system was used to increase the intracellular level of Cbl for incorporation into HgcA during expression. When compared to a truncated HgcA-1-175 construct expressed in a similar manner, the truncated variant did not co-purify with a significant amount of Cbl incorporation – we suggest that this indicates the full-length protein is structurally required for cofactor binding, though it may or may not directly interact with the bound Cbl. The FL-HgcA UV-visible spectrum exhibited an unusual and broad feature centered at ~412nm which could not be correlated to a known Cbl spectrum. No EPR signal was detected in the as-purified, aerobic protein, but this heterologous expression and detergent extraction can hopefully be optimized to

generate a robust production method for subsequent studies of HgcA bound to "base-off" corrinoid cofactor.

4.2 Future Directions

The work presented in this dissertation represents a scratch in the surface of our understanding of *hgcAB*-mediated Hg methylation. Though *in vivo* studies have strongly indicated the direct involvement of HgcA and HgcB in the Hg methylation reaction[7,8], an *in vitro* assay showing this functionality would definitively show that HgcA and HgcB comprise the minimal components necessary for MeHg biosynthesis. Such a functional assay would necessitate the generation of MeHg, which is highly toxic and dangerously volatile. Additionally, it is unknown whether an equilibrium HgcAB reaction could utilize $MeHg^+$ as a substrate and generate dimethylmercury, which exhibits even greater toxicity and membrane permeability. Our collaborators at Oak Ridge National Laboratory routinely generate and quantify these Hg species using established and safe methods, so, though care must be taken, this functional assay is within reach now that methods for HgcA and HgcB expression have been established.

A further hypothesis concerning the *in vitro* stability and solubility of HgcA and HgcB is that the two proteins form a complex *in vivo* – this is based on the fact that they appear "side-by-side" in genomes in which they are found, are not found encoded without the other, and, in a few examples, are found as a single fusion gene[9]. We also observe charge complementarity, indicating potential for electrostatic interaction, between the theoretical isoelectric points (pI) of the HgcA and HgcB constructs we study from *Desulfovibrio desulfuricans* ND132: the soluble region of HgcA has a theoretical pI of 10.0 whereas that of HgcB is 6.7. Pull-down assays in which an affinity tag is encoded at the terminus of HgcA or HgcB have been attempted by our collaborators, but hampered by the low level of HgcAB expression in native organisms. Heterologous co-expression of these genes could indicate whether they co-purify or improve the *in vitro* solubility of either protein – though no results are presented in this work, we have also constructed plasmids to test the effect of this co-expression on the solubility of HgcA and HgcB which we hope will provide insight into the HgcA:HgcB interaction. A structural model of HgcA and HgcB, derived from protein homology and structure prediction, has been computationally developed by our collaborators and provides a starting point for mutagenesis studies which could probe specific predicted interactions at the HgcA:HgcB interface.

The "base-off, Cys-on" HgcA corrinoid coordination environment is hypothesized to allow catalysis at the Co center which has not been seen in a biological system, namely the transfer of a methyl anion species[10]. Spectroscopic determination of the HgcA corrinoid coordination environment will provide insight into the chemical mechanism and inform the nature of Co-C bond dissociation. Specifically, the Co oxidation state following single-turnover methyl transfer to Hg(II) could be easily identified by EPR and would provide insight into the mechanism of methyl transfer. Of course, structural information concerning the corrinoid binding site, derived from X-ray crystallographic or extended X-ray absorption fine structure (EXAFS) data would be extremely valuable to mechanistic study.

More broadly, the biological functions of HgcA and HgcB are yet unknown: is there an as-yet unidentified benefit that MeHg production confers a host microorganism? Or do these genes play a primary role in carbon metabolism and adventitiously convert Hg(II) to MeHg? Proteomic studies have identified some differential expression in *hgcAB* deletion mutants, but this has yet to be investigated further[1,2]. Bioinformatic insight into these differentially expressed pathways could perhaps yield candidates for *in vivo* mutagenesis to determine partners of HgcA and HgcB critical to Hg methylation. We hope that (1) an understanding of the mechanism of this reaction and its catalytic efficiency and (2) the identification of other pathway components (electron donor, methyl donor, uptake and export processes, etc.) will provide answers to these overarching questions about the role of HgcA and HgcB in their microbial hosts.

4.3 References for Chapter 4

(1) Qian, C.; Chen, H.; Johs, A.; Lu, X.; An, J.; Pierce, E. M.; Parks, J. M.; Elias, D. A.; Hettich, R. L.; Gu, B. Quantitative Proteomic Analysis of Biological Processes and Responses of the Bacterium *Desulfovibrio Desulfuricans* ND132 upon Deletion of Its Mercury Methylation Genes. *Proteomics* **2018**, 1700479.

(2) Qian, C.; Johs, A.; Chen, H.; Mann, B. F.; Lu, X.; Abraham, P. E.; Hettich, R. L.; Gu, B. Global Proteome Response to Deletion of Genes Related to Mercury Methylation and Dissimilatory Metal Reduction Reveals Changes in Respiratory Metabolism in Geobacter Sulfurreducens PCA. *J. Proteome Res.* **2016**, *15* (10), 3540–3549.

(3) Nakamura, M.; Saeki, K.; Takahashi, Y. Hyperproduction of Recombinant Ferredoxins in *Escherichia Coli* by Coexpression of the ORF1-ORF2-*IscS-IscU-IscA-HscB-Hs cA-Fdx*-ORF3 Gene Cluster. *J. Biochem.* **1999**.

(4) Lanz, N. D.; Blaszczyk, A. J.; McCarthy, E. L.; Wang, B.; Wang, R. X.; Jones, B. S.; Booker, S. J. Enhanced Solubilization of Class B Radical S-Adenosylmethionine Methylases by Improved Cobalamin Uptake in Escherichia Coli. *Biochemistry* **2018**, *57* (9), 1475–1490.

(5) Denisov, I. G.; Sligar, S. G. Nanodiscs in Membrane Biochemistry and Biophysics. *Chem. Rev.* **2017**, *117* (6), 4669–4713.

(6) Ledwidge, R.; Patel, B.; Dong, A.; Fiedler, D.; Falkowski, M.; Zelikova, J.; Summers, A. O.; Pai, E. F.; Miller, S. M. NmerA, the Metal Binding Domain of Mercuric Ion Reductase, Removes Hg 2+ from Proteins, Delivers It to the Catalytic Core, and Protects Cells under Glutathione-Depleted Conditions.

Biochemistry **2005**, *44* (34), 11402–11416.
(7) Smith, S. D.; Bridou, R.; Johs, A.; Parks, J. M.; Elias, D. A.; Hurt, R. A.; Brown, S. D.; Podar, M.; Wall, J. D. Site-Directed Mutagenesis of HgcA and HgcB Reveals Amino Acid Residues Important for Mercury Methylation. *Appl. Environ. Microbiol.* **2015**, *81* (9), 3205–3217.
(8) Parks, J. M.; Johs, A.; Podar, M.; Bridou, R.; Hurt Jr., R. A.; Smith, S. D.; Tomanicek, S. J.; Qian, Y.; Brown, S. D.; Brandt, C. C.; et al. The Genetic Basis for Bacterial Mercury Methylation. *Science (80-.).* **2013**, *339* (March), 1332–1336.
(9) Podar, M.; Gilmour, C. C.; Brandt, C. C.; Soren, A.; Brown, S. D.; Crable, B. R.; Palumbo, A. V.; Somenahally, A. C.; Elias, D. A. Global Prevalence and Distribution of Genes and Microorganisms Involved in Mercury Methylation. *Sci. Adv.* **2015**, *1* (9), 1–12.
(10) Zhou, J.; Riccardi, D.; Beste, A.; Smith, J. C.; Parks, J. M. Mercury Methylation by HgcA: Theory Supports Carbanion Transfer to Hg(II). *Inorg. Chem.* **2014**, *53* (2), 772–777.